OBSERVATIONS OF JOINTS PRESENT IN THE LAWTON CLAY MEMBER OF THE VASHON STADE, EXPOSED AT A COASTAL BLUFF IN DISCOVERY PARK, SEATTLE, WASHINGTON

Amanda Dovinh Ong

A report prepared in partial fulfillment of the requirements for the degree of

MASTERS OF EARTH AND SPACE SCIENCES: APPLIED GEOSCIENCES

UNIVERSITY OF WASHINGTON

JUNE 2016

Project Mentor:
Kathy Troost

Reading Committee:
Dr. Juliet Crider
Dr. Joanne Bourgeois

MESSAGe Technical Report Number: 038

ABSTRACT

The southwest-facing coastal bluff present at Discovery Park, Seattle, Washington, displays distinctive joints throughout the exposed Lawton Clay Member. Exhibiting a characteristic local stratigraphy of permeable advance outwash over the impermeable proglacial lacustrine clay, this bluff is located in an area of Seattle at high risk from landslides. This project addressed the relationship between the joints observed at this coastal bluff and the coherency of the bluff as a whole, through remote sensing and field measurements. Aerial drone photography taken of the bluff was processed through a photogrammetry software to produce a 3-dimensional Structure from Motion model, allowing for a digital manipulation and broad examination of the bluff not possible by foot. Stereonet plots produced from these measurements provided insight into patterns of varying joint strike along a horizontal transect of the observed bluff face. Taken together, these two visualizations provided a better picture of the possible chicken-and-egg interaction of the joints and bluff topography; they demonstrated the likelihood that the joint formation at the bluff was most likely to be primarily influenced by the local topography of the bluff over other sources of possible tensional stress in the immediate area.

TABLE OF CONTENTS

LIST OF FIGURES

ACKNOWLEDGEMENTS

A great thanks to Dr. Juliet Crider and Ms. Kathy Troost, the Program Director and Program Coordinator of the Masters in Earth and Space Sciences; Applied Geosciences (MESSAGe) Program, respectively, for their academic guidance and suggestions as my mentors. I'm grateful to Kathy Troost especially for the opportunity to work on this project as my program internship, and Dr. Crider for her help in narrowing the focus and direction of my research to something manageable. In addition to Dr. Crider, I thank Dr. Jody Bourgeois for being a part of my reading committee, and Mr James Bush for my peer review and assistance with initial edits. Mr. Tait Russell proved to be an invaluable help in seeing this project through to the end, and I can't thank him enough for allowing me access to his personal drone and technical expertise with Structure from Motion. I also thank my parents, Toan and Mary Ong, and my extended family for their continued support through my academic studies.

1.0 INTRODUCTION

The intent of this project is to determine the relationship of the joints present in the Lawton Clay, as exposed at a coastal bluff in Discovery Park, Seattle, Washington, to the general shape of the bluff itself through a combination of field measurement and remote sensing. There are two main scenarios to be addressed: 1) Is it accurate to consider these joints representative of the frequency and prevalence of such fractures elsewhere in the unit? 2) What is the origin of these joints, and are these observed joints a direct result of the topography of the bluff and erosive conditions contributing to a distinct pattern of failure? If the former, this study seeks to consider the general significance of these joints as potential zones of increased groundwater movement through an otherwise-impermeable unit from the overlying aquifer. If the latter, what precise processes contribute to consistent forms of bluff failure, and is it appropriate to take these failure planes as indicative of further failures within the Lawton Clay as a whole? Examining the orientation of the joints relative to the orientation of the bluff may provide insight into greater joint-related patterns of bluff failure at exposures of the Lawton Clay elsewhere in the Puget Sound.

2.0 BACKGROUND

The observations and analyses in this report are primarily focused upon the widespread, if locally clustered jointing across the study site with the intent of interpreting the possible origin of these joints. Of particular interest is the fact that these joints are present in exposures of glacial lacustrine clay and transitionary lenses of clay/silt/sand. Hencher (2012) and Selby (1993) both define joints as discontinuities in rock, distinguished from faults by the lack of displacement along a plane parallel to the joint surface. Hencher (2012) emphasizes that joint formation—including orientation, roughness, persistence, and structure—depends upon conditions of local stress and other factors such as material strength and water pressure. He outlines three forms of joint development: primary, from the original formation stresses of the geologic unit; secondary, from the tectonic and gravitational deformation; and tertiary, from the geomorphological stresses and local weathering. Primary formation stresses can be ruled out for the joints in the Lawton Clay, since the joints at the study site cross-cut fine-grained planar-bedded glacial deposits. Thus, two possible joint origins remain: tectonic or geomorphic/weathering stresses.

The study site is also an area of rapid erosional change; general visual observations spaced over the course of a year support the hypothesis that the study site is prone to a combination of sliding, blocky, and sheet failures. Although the origin of the joints along which these failures occur will be discussed later in the body of the paper, further visual observations of water draining out of the transitionary contact between the overlying sand unit and underlying clay unit may indicate conditions where the secondary hydraulic conductivity of the clay unit may control the rate of groundwater movement through that portion of the bluff, in addition to compromising the stability of the bluff along wetted fracture planes. Stephenson et al. (1988) note that the difference between the hydraulic conductivity of unweathered and fractured lacustrine silt and clay glacial deposits can be upwards of 5 orders of magnitude; the hydraulic conductivity of unweathered lacustrine silt and clay ranges between $10^{-4} – 10^{-8}$ m/day, while the fractured hydraulic conductivity ranges between 10^{-3} and 10^{-6} m/day. Selby (1993) describes water-infiltrated mudrocks and other fine-grained deposits to be subject to the weakening of diagenetic bonds; taken in conjunction with the “softening” of the material that occurs when water content increases in the apertures of joints, the presence of water may exacerbate the failure rate of the joints at the study site, or possibly obscure the source of the original joint formation stresses.

2.1 Study Site

The site of interest is a southwest-facing, northwest-to-southeast trending coastal bluff located at the southern beach of Discovery Park in Seattle, Washington (Figures 1 and 2). Discovery Park is a converted military base. Initially developed as Fort Lawton, the base occupied most of the northwestern area of Magnolia Bluff; although it was infrequently used for military training, it never grew into the major military installation it was originally planned to be, and was subsequently purchased by the City of Seattle for the express purpose of creating parkland in the area (City of Seattle, 2007). Currently, the park houses the West Point water treatment facility adjacent to the northern beach and the Daybreak Star Indian Cultural Center in addition to fields, a residential historical area, forested trails, and rocky beaches that are popular with the public year-round. The park is bordered by the neighborhood of Magnolia, an area known for its steep bluffs, and also for its susceptibility for landslides. The Holiday Storm of 1996 – 1997 triggered a large landslide at Perkins Lane in the Magnolia neighborhood near Discovery Park, taking out four homes and a significant portion of the road (Shipman, 2001). Large, highly destructive landslides have occurred at Perkins Lane before, notably in 1968 (Tubbs and Dunne, 1977). Along with Perkins Lane, the areas of West Point and Discovery Park have been noted to be zones of persistent geologic instability, particularly responsive to potential seismic stresses via significant landslide hazard discussed further below. In light of the 1996 – 1997 landslides in particular, the Seattle Public Utilities department commissioned the comprehensive Seattle Landslide Study (Shannon & Wilson, 2000) which generated a database of 1,326 landslides dating back as far as 1890.

2.2 Local Geologic Setting

The study site is in the city of Seattle, which is located within the Puget Lowland of Washington State; The Puget Lowland is an arcuate basin between the Cascade and Olympic mountain ranges, opening to the north towards Canada and the Strait of Juan de Fuca (Galster and Laprade, 1991). The Puget Lowland is subject to complex tectonic stresses from the active interrelationships between the oblique subduction of the Juan de Fuca plate beneath the North American continental plate, the north-lateral movement of the Pacific plate along the San Andreas Fault, and the extension of the Basin and Range Province east of the area (Booth et al., 2004). Throughout the Cenozoic, the resulting northeast rotation of the coastal west of Washington State relative to the stable continent and the resisting craton of southwestern Canada has resulted in a series of east-west and southeast-northwest folds and faults from the north-south crustal shortening (Lamb et al, 2012; Wells et al., 1998). Quaternary glacial deposits up to 2000 feet thick dominate the surface stratigraphy of the area, in a discontinuous series of deposits from alternating glacial and interglacial periods (Borden and Troost, 2001).

Exposed at the Discovery Park bluff are two units of primary interest: the Lawton Clay and Esperance Sand. The impermeable Lawton Clay underlies the Esperance Sand, which is the most widespread, permeable deposit in the Puget Lowland, with free-flowing groundwater normally present throughout the unit (Shannon & Wilson, 2000). The exposure of interest at Discovery Park belongs to the Vashon Stade of the Frasier Glaciation; the glacier occupied the Puget Lowland 15-13ka (Thorson, 1979). The initial deposition of the Lawton Clay is attributed to the blockage of the Puget Lowland drainage into the Strait of Juan de Fuca by the Puget Lobe of the Cordilleran ice sheet approximately 15ka; the resulting proglacial lake drained southwards into Grays Harbor, and accumulated widespread deposits of silt and clay (Mullineaux et al., 1965). The continued southwards movement of the Puget Lobe deposited the overlying proglacial fluvial sand of the Esperance Sand. Mullineaux et al. (1965) produced approximate ages for each unit, generated from a radiocarbon analysis of peat and woody debris from the immediate Seattle area: both units were deposited within the range of 15 – 13.5ka, although as Troost and Booth (2008) cite from Porter and Swanson (1998), the limiting ages of both units was 15 – 14.5ka.

Savage et al. (2000) presents a general stratigraphic section that places the depositional representatives of the Vashon Stade in order from the bottommost proglacial lacustrine clay, to the overlying advance outwash, to the uppermost lodgement till (Figure 3). These are the Lawton Clay, Vashon Advance Outwash (Esperance Sand), and Vashon Till members. Figure 4 shows the relative stratigraphy of the beds at the Discovery Park bluff, as roughly marked out on a photograph; the lower boundary of the Lawton Clay is conformable with the nonglacial Olympia beds beneath (Galster and Laprade, 1991). The boundary between Lawton Clay and Esperance Sand is not definitive. Tubbs and Dunne (1977) cite Mullineaux et al. (1965) for the observation of a transition zone between the two units, typically consisting of an interbedded sand and clay deposit. Tubbs and Dunne (1977) support Mullineaux et al.'s (1965) observations that whereas the transition zone would technically lie within the boundaries of the Esperance Sand in regards to the type section and stratigraphic description, the same zone is better fit to be mapped and examined when considered as the uppermost section of the Lawton Clay. Thus, the contact between the Lawton Clay and the Esperance Sand as marked in Figure 4 was determined to fall at the upper boundary of these transition units. According to Mullineaux et al. (1965), the approximate thicknesses of the Lawton Clay, the clay/silt/sand transition zone, and the Esperance Sand are 70ft, 80ft, and 100ft respectively at the Fort Lawton type section. Galster and Laprade (1991) note that although the Lawton Clay at the type section location has a precise thickness of 82ft (25m), it could range between 0 and 100ft (30m) at other exposures in the Puget Lowland.

Supplemented by the full unit description of the Lawton Clay from Mullineaux et al. (1965), my observations of the Lawton Clay indicate that it is dark-grey laminated and ripple-marked clay interbedded with lighter-grey silt with a very stiff-to-hard density, with a unit thickness upwards of 30 meters. Fallen blocks of well-dried Lawton Clay fracture easily along bedding planes; of particular interest is the noted presence of vertical fractures listed under qualities that would affect the permeability of the unit (Troost and Booth, 2008). The conjugate joints that Mullineaux et al. (1965) observed as being spaced within a few inches of each other were only present with high density at the driest northwestern corner of the exposure; otherwise, they were spaced sparsely along the bluff.

The Esperance Sand is a well-sorted, fine-to-medium sand and gravel deposit locally interbedded with silt, clay, and peat lenses (Troost and Booth, 2008). As exposed at Discovery Park, Mullineaux et al. (1965) describe the unit as loose, well-sorted, medium-grained cross-bedded sand containing three silt beds and rounded fragments of clay and peat. The transition zone—fine-to-medium horizontally-bedded sand interbedded with grey clayey silt—between the Esperance Sand and the Lawton Clay is typically attributed to the Esperance Sand in stratigraphic descriptions.

2.3 Local Geologic Hazards

The study site is at risk from a number of geologic hazards. Seismic activity in the Puget Lowland is primarily attributed to the stresses generated from the subduction of the Juan de Fuca plate and the north-south shortening from the Basin and Range extension to the south; the rigid, mafic basement 25-30km below the area undergoes brittle deformation (Troost and Booth, 2008; ten Brink et al., 2002). The Seattle fault zone is an example of an active tectonic structure in the Puget Lowland, extending roughly east-west directly through downtown Seattle in a swath 4 – 7km wide and 60 – 65km long (Troost and Booth, 2008; ten Brink et al., 2002). Landslides are common in the area, often featuring an interaction between anthropogenic modifications, high-permeability deposits overlying low-permeability deposits, steep slopes, abundant colluvium, coastal wave undercutting, and seismic initiation triggers (Troost and Booth, 2008).

Magnolia, where Discovery Park is located, is not the only area prone to dramatic slope failure; several neighborhoods around Seattle have significant landslide risk (Allstadt and Vidale, 2012). Savage et al. (2000), attribute the landslide frequency in Seattle to the characteristic glacial stratigraphy of the Puget Lowland which results from several phases of Quaternary glaciation. They write that these units are "often overconsolidated, have a wide range of hydraulic conductivities, are laterally heterogeneous, and form steep, landslide-prone coastal bluffs." Most slope failures around Seattle occur in or near the contact between the Esperance Sand and the underlying Lawton Clay (Schulz 2004, 2005, and 2007). These failures have been mapped extensively; Schulz (2004, 2005, and 2007) focuses primarily on mapping historical landslides and current landslide susceptibility in Seattle using bare-earth DEMs generated from Light Detection and Ranging (LiDAR) imagery, but not with other forms of remote sensing. He has produced multiple susceptibility maps for the Seattle area, such as ones presented in Figures 5 and 6.

The study site at Discovery Park's South Beach bluff has a profile characteristic of many other high bluffs in the Puget Sound; the contact between the permeable Esperance Sand and impermeable Lawton Clay is marked by a mid-slope bench that widens from upslope failure caused by water saturation at the contact (Shipman, 2004; Harp et al., 2006; Figure 7). Tubbs and Dunne (1977) examined the study site in detail in a geologic hazards field guide generated for the Geological Society of America Annual Meeting. They attribute the frequent landsliding and erosion at the bluff to be the result of wave erosion, strong southerly winds, and groundwater movement at the Esperance Sand/Lawton Clay contact. Upper slump failure at the bluff is primarily due to this groundwater presence; the downward percolation of groundwater through the Esperance Sand is diverted at the impermeable contact of the uppermost laterally-extensive beds of the Lawton Clay, and thus moves laterally until it intersects with an exposed slope (Tubbs and Dunne, 1977). According to them, this is one of the direct contributors to the rapid destabilization and retreat of the upper bluff, which eventually causes the formation of a bench at the elevation of the impermeable contact. Tubbs and Dunne (1977) further suggest that the slumping at intercalations of sand in the uppermost section of the Lawton Clay instead of at the larger impermeable contact is due to the effects of pore pressure within the beds.

2.4 Prior Work on Joints in the Lawton Clay

Both Mullineaux et al. (1965) and Tubbs and Dunne (1977) worked at Discovery Park, primarily to characterize the well-exposed stratigraphic section seen at the South Beach bluff. Mullineaux et al. (1965) sought to "describe and divide the Lawton Formation of previous usage" from the prior nomenclature; previously, the Esperance Sand and the Lawton Clay were considered to be one unit, with a "clay phase" and a "sand phase" (Figure 8). Tubbs and Dunne (1977) sought to describe the general landslide hazards in the immediate Seattle Area, approaching their description of the coastal bluff primarily as a sum-of-factors that contributed to past slope failures at the site, with the primary contributor to slope failure being the high pore-pressure conditions generated by groundwater at the contact between the Esperance Sand and the Lawton Clay. Although Mullineaux et al. (1965) mention the presence of "conjugate joints" in their unit description of the Lawton Clay, Tubbs and Dunne (1997) do not note joints in their field guide, and neither Mullineaux et al. nor Tubbs and Dunne discuss the significance of the joints upon the general shape of the bluff, or vice versa. Harp et al. (2006), along with many others, cite Tubbs (1974, 1975, and 1977) when generating illustrative figures such as the one in Figure 7 and for the now-commonly accepted theory that landsliding in these units is strongly influenced by the buildup of water at the permeable/impermeable contact between the Esperance Sand and Lawton Clay.

Galster and Laprade (1991) suggest in their unit description of the Lawton Clay that the conjugate joint sets mentioned by Mullineaux et al. (1965) were the result of loading-related destressing after deglaciation, but do not expand upon the identity or work of the investigators who proposed this hypothesis.

3.0 METHODS

In order to examine the hypotheses of joint origin at the bluff, I intended to generate and georeference a 3-dimensional digital model of the bluff to which I could compare stereonet plots produced from the joints measured at the site. To do this, I made manual observations of the joints and study site, collected aerial photography, and took GPS points. However, various physical and technical limitations prevented me from completing all the analyses initially planned.

3.1 Fieldwork

Fieldwork was conducted in late spring during days of fair, dry weather. Foot access to the field site was via a steep trail off of the main loop trail, a short 10-minute walk from the south parking lot. This path is visible in Figure 2. Navigating the trail down to the bench level took another 10 minutes through dense underbrush. In addition to work at the bench-level, one day of fieldwork was conducted at beach-level for the purpose of collecting aerial photography.

The winter of 2015-16 was wet and warm, resulting in a burst of early springtime vegetation growth which limited my ability to access certain parts of the research site. There was a dense presence of horsetail fern, which indicates a significant amount of water in the surface soil. There was ponding at some areas of the bench, and seepage emerging at various points in the bluff at the clay/sand interface.

Figure 9 shows a large fractured corner wedge at the bluff that changed dramatically over the course of months, most likely due to the combination influence of increased water movement throughout the slope and failure along preexisting planes. Tubbs (1974 and 1975) theorized that landslides along the Puget Sound were the direct result of groundwater buildup. During winter, when there is an increased volume of water moving through a permeable unit, the intergranular pore pressure increases and thus reduces the coefficient of friction in the slope. This, in conjunction with the unique stresses generated by the aquifer overburden of the Esperance Sand over the Lawton Clay, result in mass failures characteristic of this area.

Fieldwork was restricted to periods of drier weather to avoid increased instability due to wet weather; however, during a field excursion on a clear day I observed a sudden sheet failure at the area shown in Figure 10, indicating that larger failures at this could happen at any time, even during longer stretches of dry conditions.

The approximate boundaries of the area examined for joints and photographed for the SfM model were chosen on basis of foot accessibility and bare exposure surfaces. This was to limit the scope of the area to features that I could visually verify in the field even if those areas were vertically inaccessible.

3.11 Joint Measurements

The bluff exhibits joints throughout the exposed clay unit and into the sand/clay transition zone, as seen in Figure 11. These were split into three primary groups pertaining to accessibility: 1) joints present at the upper portion of the bluff in the lower part of the Esperance Sand and sand-clay transition; 2) joints present at the middle portion of the bluff that can be visually observed; and 3) joints present at the lowest portion of the bluff at bench level that can be easily measured by hand without use of additional

equipment. Due to safety concerns, the use of rappelling equipment to measure the joints in the middle and uppermost areas of the bluff was prohibited by the Seattle Parks and Recreation Department. Measurements of the remaining joints were further limited by the risk of falling blocks of material and steep, crumbly talus slopes of fine silt, clay, and sand. Some joints, although present at the base of the upper bluff, were not accessible because of a talus slope too unstable to climb safely.

Every joint that could be accessed from the top of the talus was measured. Hand measurements of the joints present were taken using a Silva Ranger CL compass, set to the local magnetic declination of 16.5° east. General observations were taken of aperture, infilling, weathering, seepage, and modes of failure. Strikes and dips were measured according to the "right hand rule": a flat, extended right hand is oriented parallel to the plane measured, with the fingers pointing in the direction of downward dip. The direction of the thumb then indicates the strike orientation. Observations of the bluff were taken along the length of an inch-feet and decimal-feet tape measure. This 300-foot tape measure was strung out along the base of the upper bluff at the top of the talus slope where possible, but due to the irregularly increasing elevation of the top extent of the talus slope from the northwestern extent to the southeastern extent of the study range, the horizontal accuracy of the tape measure was approximate at best (Figure 12). The length of the bluff necessitated the relocation of the tape towards the southeast and upslope on the talus surface, so the tape had to be moved several times and the distance recalculated; these measurements were converted to meters for the purpose of Table 1 in the appendix and for the observations in the Results section. Hand measurements were taken where possible; this was usually at the top of the talus slope at the direct base of the bluff surface, underneath overhanging, fractured material. This meant that horizontal distance measurements of the joints were taken more parallel to the generalized slope of the talus contact with the bluff face rather than to the planar beach surface or to the irregular base level of the bench, and thus the distribution of the features recorded in Table 1 may not accurately represent the true horizontal distribution.

Measurements of strike and dip were taken without the use of a bubble level, although these numbers were observed as close to a level standard as possible by hand. Most exposed, observable surfaces were planar or required some scraping to remove surface material, but some were irregular even after cleaning. Where space allowed, the flat cover of my field book was used as an even surface from which to measure dip. Where the joint surface was too small or shallow to use my book, a best visual approximation was made of the area most accurately representative of the joint dip and measurements were taken from there.

3.12 UAV Survey

Photographs for the digital model were taken by UAV (Unmanned Aerial Vehicle, or drone). The UAV survey was on March 30th and began at 3pm, in sunny, windy conditions. Tait Russell, a recent graduate from the University of Washington, provided the equipment and technical support, piloting his recreational civilian drone to take aerial photography with the intent to help me develop a Structure from Motion (SfM) model. SfM is new, relatively inexpensive approach in the field of photogrammetry, which utilizes photography to remotely survey and map objects of interest. SfM allows for the automated construction of a 3-dimensional digital model of the photographed surface, which can then be exported as a Digital Elevation Model (DEM) once georeferenced through the use of GPS points or other Ground Control Points (GCPs) (e.g. Russell, 2016). Photogrammetry via the use of a UAV was first conducted in 1979, and the first high-resolution Digital Terrain Model generated from UAV photography was done as recently as 2005 (Niethammer et al. 2012).

Low tide, at 4:30pm, allowed us set up the drone far enough away on the beach from the bluff to visually assess the entirety of the area to be photographed. Figure 13 shows the lateral extent of the area that was

modeled, from the landslide bowl at the northwestern end of the bluff and the vegetated gully at the southeastern end.

Tait piloted a DJI Phantom 2 Vision+ equipped with a 14-megapixel camera. The drone's three rechargeable batteries allowed for approximately 45 minutes of flight time, which we subdivided into three 15-minute flights focusing on the different areas of the bluff. The first flight covered the general scope of the bluff from each side of the boundary marked in Figure 13. The drone was controlled by a combination remote and phone application that allowed Tait to view the images from the drone as they were taken, allowing him to more clearly focus on the areas I described as most crucial to model. The second and third flights were close-ups of each respective half of the bluff, focusing primarily on the sheer bluff surfaces and not on the vegetated bench. The photos were taken continuously in a JPEG format, at a rate of one picture every three seconds.

3.13 Trimble Geo7x GPS Measurements

A total of 12 GPS points were taken at various points along the bench and at the upper treeline. These points were necessary to provide a geographic reference frame for the completed SfM model, and were split up into two files: 9 bench-level points spread out on the lower surface and 3 treeline points placed at the base of distinctive trees at the very edge of the upper bluff. These points were collected using a Trimble Geo7x GPS receiver and transmitter in conjunction with a Zephyr Model 2 external antenna. I recorded data at each location until the average accuracy of all the points was reported by the instrument to be within 15cm or better. Photos of the control points are included in the appendix.

3.2 Post-processing

Post-processing of the field data involved a stereonet analysis of the measured joint orientations and the development of a Structure from Motion model from the drone photographs taken. The stereonet program used was Stereonet 9.5.3 (Allmendinger, 2016). The Trimble GPS points were intended to georeference the SfM model, but unforeseen complications during the data collection phase prevented differential corrections from being done. Without corrected GPS, I could not georeference the SfM model; this would not have been possible even with corrected GPS, due to the amount of vegetation and bench-level blurring that obscured the exact areas where I collected points. More information regarding the GPS errors are located in the appendix.

Before the photographs taken by the drone could be used to generate the SfM model, they required some pre-processing. I followed the processing procedure described in Russell (2016) with further advice from Tait himself. The drone collected inaccurate GPS information, stored as geotags attached to each photograph. These must be removed otherwise the SfM processing software Agisoft PhotoScan Pro (v. 1.2.3) may misalign the photographs and produce a deformed model. Russell (2016) recommends EXIFtool to remove the geotags. These adjusted photos were then loaded into a new project in Agisoft Photoscan Pro; this program was run on a Dell Precision Tower 7000 Series desktop computer, equipped with two Intel Xeon hyper-threading 6-core processors for a total of 12 cores with the capability of 24. With 64 gigabytes of RAM and two graphics cards (GeForce GTX 70 Ti and Quadro 4000), this computer was the most powerful that I could access for modeling.

There were two main modeling steps completed in Agisoft Photoscan Pro. The first was to generate a point cloud made of the feature patterns found in the aligned photographs, called a sparse point cloud. This was done by first adjusting the photo alignment to the high accuracy setting, changing the photograph selection to generic, and increasing the maximum threshold of detected patterns in each

photograph to 400,000 from the default 40,000 and the maximum threshold of corresponding patterns in other photographs to 10,000 from the default 1,000 per Russell's (2016) steps. Once the sparse point cloud was completed, the second step was to generate a dense point cloud. The difference with the dense point cloud is that whereas Agisoft Photoscan Pro detected and correlated patterns in the photography to generate the sparse point cloud, the dense point cloud is made by utilizing the estimated camera positions and the approximate depth to surface, resulting in a smoothed, solid model. Russell (2016) suggests setting the cloud density to medium and the depth filtering to mild to reduce over-interpolation and to preserve the angularity of exposed surficial features.

Due to a lack of GPS data imported to the model as markers, building a DEM was not possible. However, an orthophoto could be built. I used the default pixel size suggested of 0.00427961 meters and allowed the program to estimate the bounding area. Likewise, when exporting the orthophoto, I kept the suggested default export pixel size of 0.00427961 meters and kept the program settings to automatically estimate the bounding area. I kept the default TIFF compression as LZW, the JPEG quality at 90, and exported as both a TIFF and JPEG file. Despite the suggested default pixel size, the resolution of the output orthophoto was unlikely to be accurate to 10^{-8}m. The orthophoto itself did not display a view of the bluff that could be easily interpreted, and was not included in this report.

4.0 RESULTS

4.1 GPS and SfM

In regards to the SfM model; although imperfect due to the lack of georeferencing, limited computer processing power, and site limitations, the resulting output was sufficiently precise in the areas of interest to be examined, and the model provides a valuable tool for freely manipulating the viewpoints of the bluff to gain a more thorough grasp on the topography.

Due to the technical issues discussed in-depth in the appendix, the results from both the GPS and SfM process were ultimately inconclusive, or produced far less workable data than originally planned. The GPS points were not able to be differentially processed; without corrected points to export and georeference the Structure from Motion model, a DEM could not be created and further analyzed in ESRI ArcGIS. However, considering the ability of Agisoft Photoscan Pro to manipulate the completed model into various views at various levels of zoom, the SfM model still acted as a useful tool to visually confirm physical features of the bluff that could otherwise only be seen in partial during fieldwork at either bench or beach-level.

Figure 14 is the completed model, seen from a beach view; additional images of the model from different angles are in the appendix.

4.2 Field Observations

Detailed fieldnotes are located in the appendix, along with a table of the joints measured.

The outermost portion of the bench, away from the talus-covered lower bluff face and extending to the beachside edge of the bench, exhibited a hummocky topography which was mostly hidden by a dense patch of young alders, blackberry, and horsetail. The winding trail used to descend from the trailhead at the top of the bluff down to bench level passed by audibly trickling water and over older, rotting woody

debris sunken into soft, wet mud that adjacent to visible standing water—a small pond was mostly obscured by surrounding vegetation, but was large enough to make a deep splashing sound when objects were thrown into the center. The bluff surface examined was generally near-vertical, sloping the most near the bench at the edge of the talus cone. The joints present at measurable elevations in the bluff were clustered at both far ends, and intermittently in the middle. From beach-level, there was visible, steady water trickling observed pouring down in rills and minor channels over the greyish clay-mantled underlying Olympia beds and down onto the beach.

Due to the changing conditions of moisture, vegetation, and elevation across the bluff, it was simplest to characterize the bluff in terms of general domains, separated from one another by distinguishing differences in such attributes like bluff section orientation, joint frequency, seepage, and primary talus slope material. Five domains were distinguished, and are identified in Figure 15 as domains A, B, C, D, and E.

Domain A begins at the westernmost end of the bluff and runs 20m, with an estimated bluff strike of 140 degrees. There is no obstructive vegetation to reduce the amount of sun or wind exposure at this domain, resulting in a very dry section of the Lawton Clay that resembles more coherent rock. Talus material is clay—dry, greyish tan in color, and powdery in texture. Surface color of the clay is also tan, but fresh surfaces within the bluff are dark grey, indicative of higher moisture content. A hand sample taken from the bluff was determined to be of S6 (very hard) grade weak rock and indented with difficulty by a thumbnail. It splits readily along bedding planes and fractures to powder under blows from a geological hammer; it is also relatively easy to scrape with a sharp edge. Larger joints present in this domain were spaced about 10cm – 1m apart with a distinct stair-stepping structure parallel to the bluff at the far corner (Figure 9b). The majority of the exposure was highly fractured and irregular, exhibiting small block or wedge failures. The smaller fractures had spacings of 1 – 20cm, and were oriented both perpendicular and parallel to the bluff. Some exposed joint surfaces showed red-black discolorations, further indicative of past water movement through minor apertures. Apertures themselves were minor, between 0.1 and 0.5mm between both sides of the joints and bearing no distinct chemical or detrital infilling. Small fractured blocks were easily dislodged by hand or some prying; numerous plumose structures and associated hackles were observed (Figure 16). Nearer to the boundary with Domain B, some root and insect infilling was observed, and some small plants were growing out of joint partings. Near-surface fractures in the most weathered areas and adjacent to the talus zone at bench level were more irregular, frequent, and closely spaced than upper bluff fractures, which appeared to fail in larger sheets 2 – 3 meters square rather than in smaller blocks. Nearly all fallen blocks had smooth faces and sharp edges along the planes of breakage. Upper bluff failure within this domain—and all the domains—was observed to occur at the intersection between 3 planes: an uppermost horizontal failure along bedding, an irregular perpendicular failure along a conjugate joint, and a backside sheet failure parallel to the bluff.

Domain B runs from position 20m – 60m, with an estimated bluff strike of 110 degrees. The 20m position marks a large broken corner wedge visibly separated from the upper bluff. The characteristics of Domain A and B are mostly similar; dry, tan surface exposures with powdery clay talus and smaller irregular fracturing close to bench-level, and an upper bluff area marked by larger, thicker, longer sheet fractures with an irregular perpendicular fracture plane, a smooth horizontal upper plane that failed along the bedding, and a smooth fracture plane against the bluff surface. The upper bluff appeared primarily intact, with very minor perpendicular fractures that were often covered in soil wash and organic debris from above. Most of the upper fractures appeared to be shallow and roughly parallel to the bluff face, with tight apertures only discernable by the stairstepping pattern produced by sun shadow. Fallen blocks that had broken along bedding planes exposed distinctive ripples (Figure 17). Unlike the consistently dry Domain A, Domain B marks the transition in the bluff to an in-situ increase in water content and vegetation; bench-level talus material at about 30m becomes darker grey and firm, with a greater density of larger vegetation. The gradual elevation of the top of the talus increases along the length of the tape measure,

providing access to more of the upper sandy sections of the stratigraphy. Domain B also has larger bluff failures than those present in Domain A, displaying fresh dark blocks on the bench and fallen young trees from the top of the bluff. The leaves on these toppled trees were fresh at the time of field observations and the roots were partially exposed; some were clumped together with original soil material and some were buried beneath a mixture of overhead sand and clay. Besides this fresh failure and the dry zone adjacent to Domain A, the area of Domain B closest to Domain C was covered with a significant amount of overhead dark soil wash and overgrown with lichen and moss. Removing the soil and vegetative cover revealed dark grey underlying clay, indicating water present either within the clay itself or water movement through the soil mantle sourced from overhead seepage out of transitionary sand/clay lenses.

Domain C runs from 60m – 80m, with an estimated bluff strike of 120 degrees. Domain C had significantly more moisture than Domain B; the water flowing over the surface was enough to support a mat of plant roots, with plenty of moss, lichen, horsetail, and other plants sprouting directly out of the bluff. There were few prominent or pervasive joints observed, possibly due to the lack of recent failures that would expose fresh planes, visually obstructive vegetation, and/or the reattachment of fallen clay particles onto the lower surfaces of the bluff, resulting in a dark, indistinct, nubby texture. Exposed surfaces were dark and moist, with what partings present often densely infilled with roots and moss if not infilled by reattached clay. Primary talus material was vegetation-covered dark clay mixed in with broken logs; fallen chunks of clay were blocky, but exhibited rounding of the corners and edges unlike the chunks present in most of Domains A and B. At about 75m, overhead seepage was observed coming directly out of a fracture plane running parallel to the bluff face. About 10m above the elevation of the seepage, the bluff material was drier and exhibited fewer visible joints, although vegetation cover remained. At about 80m was an exposed, dark grey portion of bluff that was missing surface vegetation; I observed a large sheet failure detach from the bluff at this location. This failure zone is featured in Figure 10. The exposed material was very moist upon immediate examination after the failure, but this failure as a whole could indicate that although the remainder of Domain C appeared to be mostly coherent, the coherency was an illusion brought about by soil cover and vegetation growth rapidly covering exposed joints and fracture planes from previous failures.

Domain D runs from 80m – 130m, with an estimated bluff strike of 125 degrees. Domain D, similar to Domain B, marks a transitionary zone between moist, mostly-clay talus and bench material into dry, mostly-sand talus and bench material. This domain is distinguished by multiple points of water seepage dripping out from the soil mantle present at 100m and 120m and by a decrease in obstructive moss and lichen across the lower portion of the bluff. Access to the bluff was limited in this domain due to the steepness of the talus; it was too unstable to climb safely and take closer measurements. 85m approximately marks the location of slightly slumped stairstepping fractures (Figure 18). The presence of these fractures support the hypothesis that the pattern of irregular, deep perpendicular joints crosscutting multiple layers of preexisting parallel joints extends through Domains A and D; joint patterns similar to Figure 18 in Domain D are found in Figure 11b from Domain A. A large corner fracture at 87m had a large sandy talus pile directly beneath the overhanging soil material; the upper portions of the bluff were thus freed of vegetation and exposed fresh surfaces that included both the Lawton Clay and some of the overlying sandy transition lenses. However, like with the remainder of the bluff within this area, it was difficult to pick out joints in the lower exposures of clay due to bumpy clay reattachment surfaces. The immediate area of the corner failure was dry, but at about 100m, enough seepage was present to support the dense sprouting of horsetail out of the surface. Here, the only lower visible failures appeared to be small sloughing movements of the clumped clayey talus material away from the main bluff face. Some of these partings were wide and deep enough that I was unable to see to the bottom; although depth was indeterminate, the talus was separated from the main bluff at widths of 1cm – 15cm. The gradual elevation increase along the very top of the bluff had become great enough at this location relative to Domain A that the presence of sandy transition lenses in the uppermost section of the clay unit became evident, distinguished from the rest of the bluff by the numerous insect burrows spotted throughout. At

about 110m, a combination of increasing vertical thicknesses of the uppermost overlying sand unit, increasing frequency of sand lenses at the transition zone between the clay and the sand, and decreasing vertical thicknesses of lower exposures of the underlying clay unit covered up by increasing thicknesses of talus contributed to medium quartz sand becoming the primary talus material on the bench.

Domain E runs from 130m – 180m, with an estimated bluff strike of 140 degrees. Domain E extends into a forested area off of the main bluff; this required navigation over steep sandy talus high above the bench; the eye-level bluff material was no longer exclusively clay. Domain E is distinguished from the other domains by being entirely within the sand/silt/clay transition zone between the Lawton Clay and the Esperance Sand. Larger measureable joints in the lower portion of the bluff were infrequent from 20 – 130m, but there were a number of accessible joint sets present in the transitionary zone. These joints extended through cross-bedded medium quartz sand and laminar-bedded silt and clay and were mostly parallel to the bluff; there were some smaller, evenly-spaced irregular fractures exhibiting red-black oxidation surfaces similar to those in Domain A. Some flat concretions observed at 170m support Mullineaux et al.'s (1965) observations of the Lawton Clay, although these concretions are located nowhere else in the bluff accessible by foot. The same problem with joint visibility was present in Domain E as it was in Domains C and D; nubbly surface textures and moss often hid or partially obscured measurable surfaces. Unlike with other domains, the bluff surface vegetation appeared to root deeper than just the overlying soil layer; some of the joints that were parallel to the bluff exhibited roots growing through the cracks and forming enough space to between the parallel sheet and the bluff to form small caves.

Figure 19 is identical to Figure 15 except where each domain is annotated with the approximate bluff strike for that domain.

4.3 Joint Orientations

Forty-five joints were measured in all, with the majority of them clustered at the far northwestern end of the bluff in Domain A. Figure 20a shows a completed stereonet with all 45 joints plotted, and Figure 20b, a plot of all the poles to the plane, shows nearly a full-180 spread of strike orientations.

As observed in the field, the joints had two major orientations relative to the orientation of the bluff surface; joints that were roughly parallel to the local strike of the bluff face (Figure 21a) and joints that were roughly perpendicular to the strike of the bluff face (Figure 21b). Joints designated "parallel" mostly strike 100 – 160 degrees. The "perpendicular" fractures show a broad distribution with no clear common strike orientation (Figure 21b), which corresponds to field observations of their relative irregularity. Due to the fact that the perpendicular/parallel determination of joint orientations were taken relative to the local strike of the bluff at which the joint was measured, some of the parallel joints in Figure 21a do not fall within the average strike of the bluff within each domain where the majority of the other joints lie. The field determination of "parallel" vs. "perpendicular" was entirely dependent on the local variation in the bluff; I noted certain joints as "parallel" if my visual assessment of the joint plane relative to the localized block from which I was measuring it was approximately parallel, but this sometimes meant that those joints might not have been parallel to the bluff in a broader view. The determination of "perpendicular" joints was likewise, but I categorized "perpendicular" joints as any joint that was not definitively parallel to the bluff. All of the dips measured were high-angle, varying between 70 – 90 degrees with a calculated average of 80°.

Figure 22 is an annotated scatterplot that shows the spatial variation of joint strike orientations; to plot strike, all values were converted to the 0 – 180 hemisphere by subtracting 180 degrees from strike values that were greater than 180. Domains A – E are subdivided in the plot by vertical blue lines, and horizontal

shading in orange and blue 10° wide, centered around the average strike values of the bluff and of the parallel joint orientations respectively.

The strike orientation patterns seen in the joints roughly correspond with the generalized strike orientations along the horizontal expanse of the bluff as seen in Figure 23, but more obviously so in Figure 22 when comparing the orange and blue strike averages. Although the range of strike values for the joints tended to be greater than the estimated, approximate strike of the bluff in which they were located, the general trend indicates that more southward-striking joints were clustered at the ends of the transect where the bluff strike was more southwards, while the joints in the center, more east-striking area of the bluff also happened to be striking more eastwards. However, as shown in Figure 23, which divides up all the joints into five separate stereonets by domain, most of the joints observed were already clustered at either end. Domain C only has one joint recorded for a horizontal span of about 20m. This is especially clear in the Figure 22 scatterplot, which more distinctly shows the clustering of joints in domain A.

The distribution patterns or lack thereof observed in these joints, although intriguing, may be the result of disproportionate statistical representation during joint measurement due to the surface conditions and accessibility limitations at various locations along the bluff; for the horizontal distance between 20m and 130m, joint measurements were few and far between. Not many joints were observed because the higher water content in this area encouraged the widespread growth of moss, lichen, and other plants over the surface of the bluff; the exposed textures of the bluff itself were complicated by the uneven reattachment of clay particles to the lower, accessible bluff area near to the bench, which may have caused the infilling or sealing of joints that would otherwise be visible. In addition, the bench material transition from primarily clayey talus to slipperier sandy talus made some stretches of the bluff manually inaccessible. I was not able to climb up the steep talus slope and stand close enough to an observed joint measure it. However, it is possible that the fewer observed joints in this horizontal range could suggest a lower frequency of joints in the sandier sections relative to the rest of the bluff.

5.0 DISCUSSION

5.1 Joint Origin Hypotheses

Hencher (2012) outlines three stress-related origins of joint formation, only two of which would apply at this site: tectonic or geomorphic/weathering. Primary origins of joint formation—resulting from the original formation stresses of the material—do not apply at this bluff because the joints crosscut bedded glacial deposits. Here, I divide the geomorphic /weathering stresses further into two mechanisms and so examine three major hypotheses regarding the origin of the joints: 1) tectonic; 2) drying or unloading; and 3) related to the topography of the bluff. Of the two joint sets observed at the bluff, the "parallel" joints show more consistency, and so it may be most worthwhile to focus on the orientations of the parallel set.

Narr and Suppe (1991) describe tectonic joints in bedded sedimentary rock to be generally oriented perpendicular to the bedding and occurring in sets of parallel fractures, but they make the claim that an outcrop usually only has one well-developed joint set. This joint set would typically be oriented perpendicular to local fold axes (Narr and Suppe, 1991), or parallel to the compression direction. The tectonic stresses in the immediate area are from north-south shortening and compression in the Washington fore arc, which are thus responsible for east-west trending uplifts, faults, and folds with north-south compressive axes (Wells et al., 1998; Galster and Laprade, 1991; and Booth et al., 2008).

Joints tend to form in tension, as extensional fractures parallel to the maximum compressive strength (Hencher, 2012). Thus, it would be expected that the parallel joint set at the bluff would be approximately north-south, perpendicular to the east-west orientation of the nearby Seattle fault system and other features. However, for the joint orientations to be indicative of larger regional stresses, I would expect that they would remain consistent for the entire exposure. Figure 21a shows that the parallel joints are oriented between 102 – 160 degrees, and dip to the southwest; Figures 22 and 23, showing the horizontal distribution of all the joints along the domains of the bluff, indicates that joint orientations did not remain consistent over the area of the observed bluff exposure. Because the joint orientations are not consistent with each other over the exposure and do not align with the expected north-south shortening direction, it is unlikely that the joints at the bluff are tectonic in origin.

Goehring (2013) describes joint sets that form under cyclical wetting/drying conditions in sedimentary deposits as typically surficial hexagonal or rectilinear contraction cracks. These are usually not found in glacial lacustrine clay deposits, but in dried mud, which itself is a mixture of clay, silt, and organic matter (Goehring, 2013). Water was definitively observed flowing through most of the bluff, either over the surface or out of joint partings close to the relatively impermeable boundary between the Lawton Clay and the Esperance Sand; the discolored joint surfaces found where no waterflow was observed indicated that water movement through the joint spaces at those areas had occurred before, and may be a reoccurring phenomenon dependent upon seasonality or other groundwater parameters. Although Domain A was distinctly dry, the cracks present were neither rectilinear nor hexagonal, and penetrated into the bluff at inconsistent depths. Of interest is the presence of multiple initiation points and the associated hackles in Domain A, showing fracture propagation outwards from a preexisting flaw; these plumose structures are generally considered to be indicative of tension stresses (Hencher, 2012; Helgeson and Aydin, 1991; Figure 16). However, Domain A had the greatest amount of irregular fracturing compared to the remainder of the bluff; the plumose structures observed did not consistently appear only in joints that corresponded to the parallel-to-bluff joint sets, but throughout the domain and oriented both parallel and perpendicular. The fracture planes, whether those were perpendicular, parallel, or irregular and in-between, did not closely resemble the fracture patterns of cracks formed from cycles of wetting and drying, and are thus unlikely to have formed under repeated desiccation periods. However, the irregularity of the closely-spaced fractures at a wide range of orientations as seen in Figure 22 could indicate that drying might have partially influenced the joint formation in Domain A (Crider, 2016, personal correspondence).

The final hypothesis is that the origin of the parallel joint set is directly related to the orientation of the bluff. Hencher (2012) makes note that tension fractures could occur as a result of the stresses generated by intergranular pore water pressure in sediment piles; sheeting joints, in particular, he defines as being directly related to the near-surface stresses generated by local topography. Hencher (2012) considers these joints to be relatively rarer in sedimentary rocks and conglomerates as compared to massive igneous rocks, but emphasizes the positive feedback between alternating failure events and erosion—weathering processes contribute to the continued development of new parallel-to-surface sheeting joints as fresh surfaces are exposed by the failure of the old slab. Selby (1993) goes into more mathematical detail; the use of a finite-element stress analysis allows for the calculation of the predicted amount of tensile deformation at an area based upon a geometric cross-sectional model of the deformable body; an examination of the nodal displacements of the geometric elements upon loading permits the analysis to determine the induced strains and stresses on the system. This analysis allows him to create simplifications of natural models, and to predict modes of failure based upon strain—he references his prior work (Augustinus and Selby, 1990) to discuss the likelihood of vertical joints forming in sheer orthoquartzite and sandstone faces as a result of tensile stresses generated by the weight of overlying material and by the differing rates of deformation between two different materials in direct contact; however, he also implies that the propagation of these near-vertical tensile joints are responsible for a

significant amount of steep slope failure and recession, thus controlling the development of the actual cliffs that are subject to this kind of stress (Selby, 1993).

Figures 22 and 23 roughly demonstrate that the parallel joint orientations change along with that of the bluff, within a range. The high-angle dips of all joints measured are reflective of the high-angle dip of the bluff itself. Given that Figures 22 and 23 show the measured joint orientations correlating roughly with the orientations of the bluff, it's likely that the tension stresses generated by the sheer bluff surface are at fault for the parallel-to-surface sheet and block failures; the near-vertical orientation of these tension joints in the horizontally-bedded Lawton Clay and the irregular nature of the perpendicular fracture planes in the uppermost, clay/silt/sand part of the bluff correspond with observations by Selby (1993) of tension joints in horizontally-bedded sedimentary rock frequently being near-vertical, and in mudrock and other weak rock as frequently curved and discontinuous. At the most exposed corner end of Domain A, where the properties of the clay more closely resembled that of rock due to the extreme dryness, failure occurred not only in sheets, but also in blocks and wedges. Elsewhere on the bluff, where more moisture was present as seepage out of the interbedded clay/silt/sand between the Esperance Sand and the Lawton Clay, failure was primarily in large sheets, parallel to the bluff. In light of this, it is less accurate to describe the parallel joints as one joint set—but rather as an approximate series of five different parallel-to-bluff joint sets corresponding to the five bluff domains where they are located.

From this, it would be inaccurate to consider these joints representative of the frequency and prevalence of such fractures in the Lawton Clay elsewhere in the Puget Lowland. Because strike orientations of the joints are not consistent across the bluff but shift accordingly as the strike of the upper bluff surface shifts, it can be inferred that the joints are a result of the unique conditions at the bluff itself. It is therefore unlikely that the joints at Discovery Park are representative of the Lawton Clay regionally. This finding suggests that bluff exposures such as this one may not provide data by which to evaluate the presence of regionally-extensive joint systems for evaluation of joint-compromised impermeability or fracture control of fluid migration in or through the Lawton Clay.

It is difficult to ascertain if the parallel joints are responsible for the bluff topography, or if the topography is responsible for the joints. In all likelihood, joint formation and bluff development are interrelated; tensile stresses acting in conjunction with pore pressures promote joint propagation and eventual sheet and block failure, but the exposure of fresh surfaces along that parallel surface opens up new surfaces to weathering and other environmental stresses which could promote a faster rate of joint formation behind the fresh surface. The presence of vegetative cover—mosses, lichens, surficial root matting, tree canopies—may impede this cycle of positive feedback, as possibly suggested by the lack of joints observed from Domains B to D, where vegetation and reattached clay provided a thin barrier between "fresh" surfaces and weathering processes. Figure 10 demonstrates that this barrier is not foolproof; despite the possible slowing of the bluff retreat due to vegetation, parallel joint development persists in the lower, clayey portion of the bluff. When considering that the large, deeper-set recent sandy failures in Domains B and D occurred at the uppermost visible stratigraphy, such parallel joints may extend to cover a large surface area set further back into the bluff than would be suggested by the numerous other instances of smaller, near-surface sheet failure occurring lower on the bluff.

5.2 Further Work

Further work at this bluff would include more precise observations of each individual joint, and minor joint set measured. For this project, I examined each joint individually, but I did not consider grouping them into minor sets such as those seen in Figures 9a and 9b. Domain classifications were determined retroactively from field notes and horizontal measurements, so concurrent field observations with field measurements could more clearly delineate the boundaries of these domains. If possible, closer

examinations of Domains B – D might be able to reveal more joints than initially observed. Collecting more joint data would allow for more precise analyses of joint orientation changes occurring alongside bluff orientation changes, and allow me to solidify the foundation of the topographic-stress hypothesis, or to possibly refute it depending on the insight these additional joints could provide.

5.21 Measuring Rate and Volume of Bluff Retreat

This coastal bluff, as seen in Figure 9, is prone to rapid, significant change over a short period of time, and thus becomes ideal as the focus of a time-lapse study on coastal erosion or of bluff evolution. If possible, a high resolution SfM model could be georeferenced with several GPS points at key, unchanging locations. This could then act as a baseline model from which to compare subsequent models georeferenced using GPS points taken at the same locations as the first. A georeferenced SfM model can be used to create a DEM, which can then be exported and manipulated in ArcGIS, allowing future researchers to conduct a mass-subtraction between the baseline and future DEM models and determine a quantifiable value of change over time. To avoid the blurring effect of vegetation upon the final SfM model, the UAV flight would ideally be conducted on a calm, dry, cloudy day during winter, when branches are bare and undergrowth is at a bare minimum. Each subsequent scan, if done yearly, would need to be done about the same time each year—but this is dependent on yearly winter conditions. Some winters may be warmer and wetter and promote more vegetation growth than is desired. Otherwise, the time-lapse focus of the model may be more suited to a smaller portion of the bluff that undergoes significant change while being mostly bare of vegetation year-round. This would be the 60m horizontal distance that spans Domains A and B.

6.0 CONCLUSIONS

A combination of remote sensing with a UAV and field observation allowed for the characterization of joints present in the Lawton Clay, as exposed at Discovery Park. These joints were present at a mid-level bench at a coastal bluff, and were observed within the Lawton Clay and the overlying Esperance Sand, as well as the sand/silt/clay transition lenses between them. Bluff failure in the form of landsliding has been noted in the immediate Puget Sound region as being oftentimes influenced by pore pressure building up in the Esperance Sands at the uppermost impermeable layer of the Lawton Clay; prior stratigraphic analyses of the Fort Lawton type section suggest that the mid-level bench was formed from this pore pressure stress causing upper-bluff failures, which led to the retreat of the Lawton Clay and overlying deposits back from the edge of the more resistant underlying Olympia Formation.

This project sought to examine the precise relationship between the observed joints and the development of the upper bluff topography at this coastal bluff, and to do so, a horizontal transect was run across the bluff that traveled from the base of the Lawton Clay up to the sand/silt/clay transition lenses, and permitted the characterization of notable domains and the measurement of joints. Joints were clustered at drier exposures and classified as either “parallel” or “perpendicular” to the bluff, but exhibited a near-360 spread of strike orientations along the length of the transect. Analyzing these joints in conjunction with bluff topography through the use of a Structure from Motion model generated from UAV photography, stereonets, and a scatterplot revealed that general patterns where the average strike orientation of the joints within each domain was closely related to the average bluff orientation of that domain.

Given this observation, I conclude that the joint formation is most closely related to the topographic influence of the bluff than it is to local tectonics or drying/wetting cycles. Due to the fact that the joint

orientations changed with the orientation changes of the bluff, this relationship could be attributed to the unique conditions of this particular bluff. and may not provide an accurate representation of joints within the Lawton Clay as a whole, or of joint formation elsewhere in other coastal bluffs formed from glacial materials. It is therefore unlikely that the joints at Discovery Park are representative of joints in the Lawton Clay, and would not be appropriate to consider as characteristic failure planes when predicting patterns of bluff failure at exposures of the Lawton Clay elsewhere in the Puget Sound.

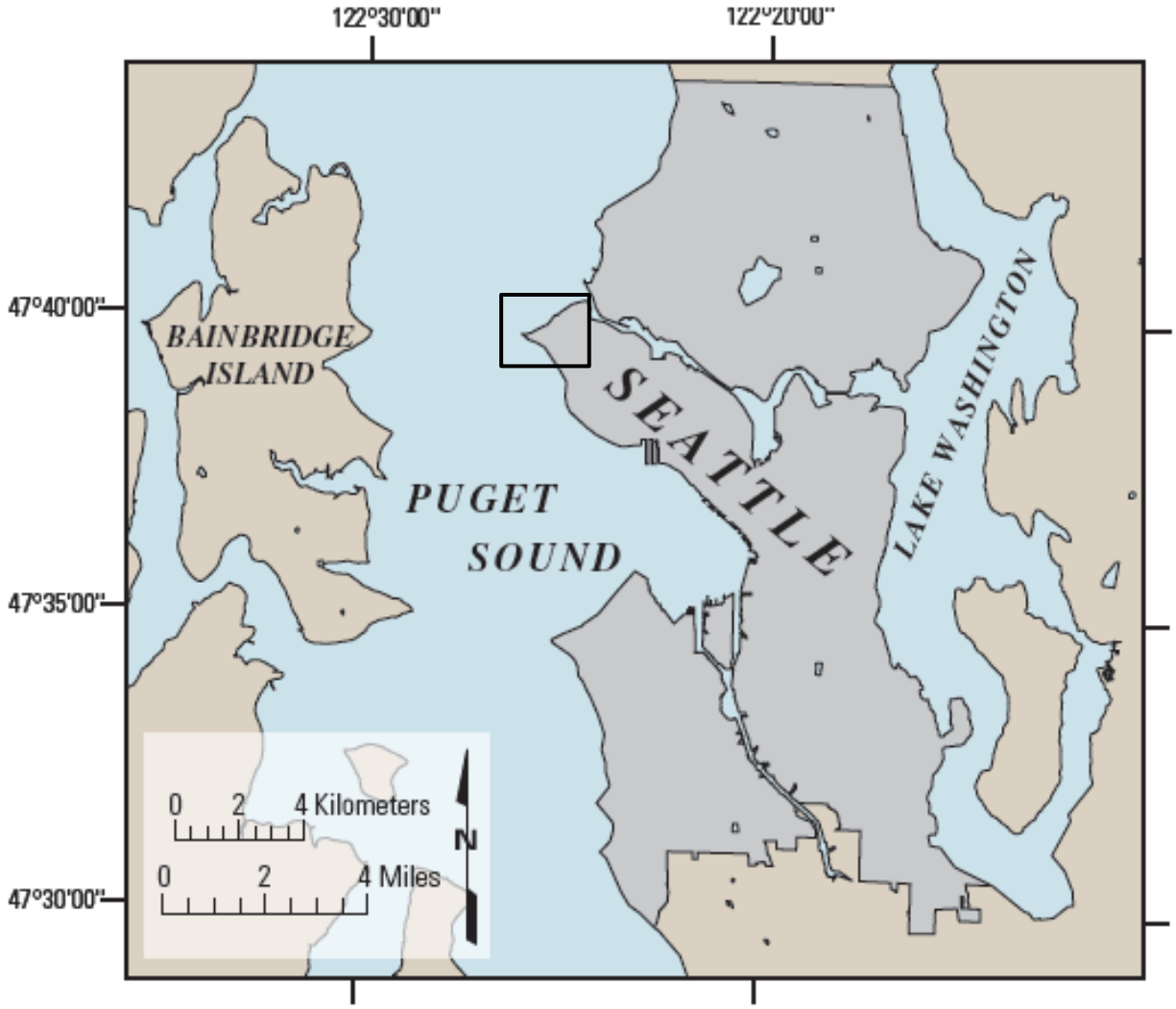

Figure 1: The Seattle area, relative to the Puget Sound, Lake Washington, and Bainbridge Island (Schulz 2004, 2005). Discovery Park is within the black rectangle.

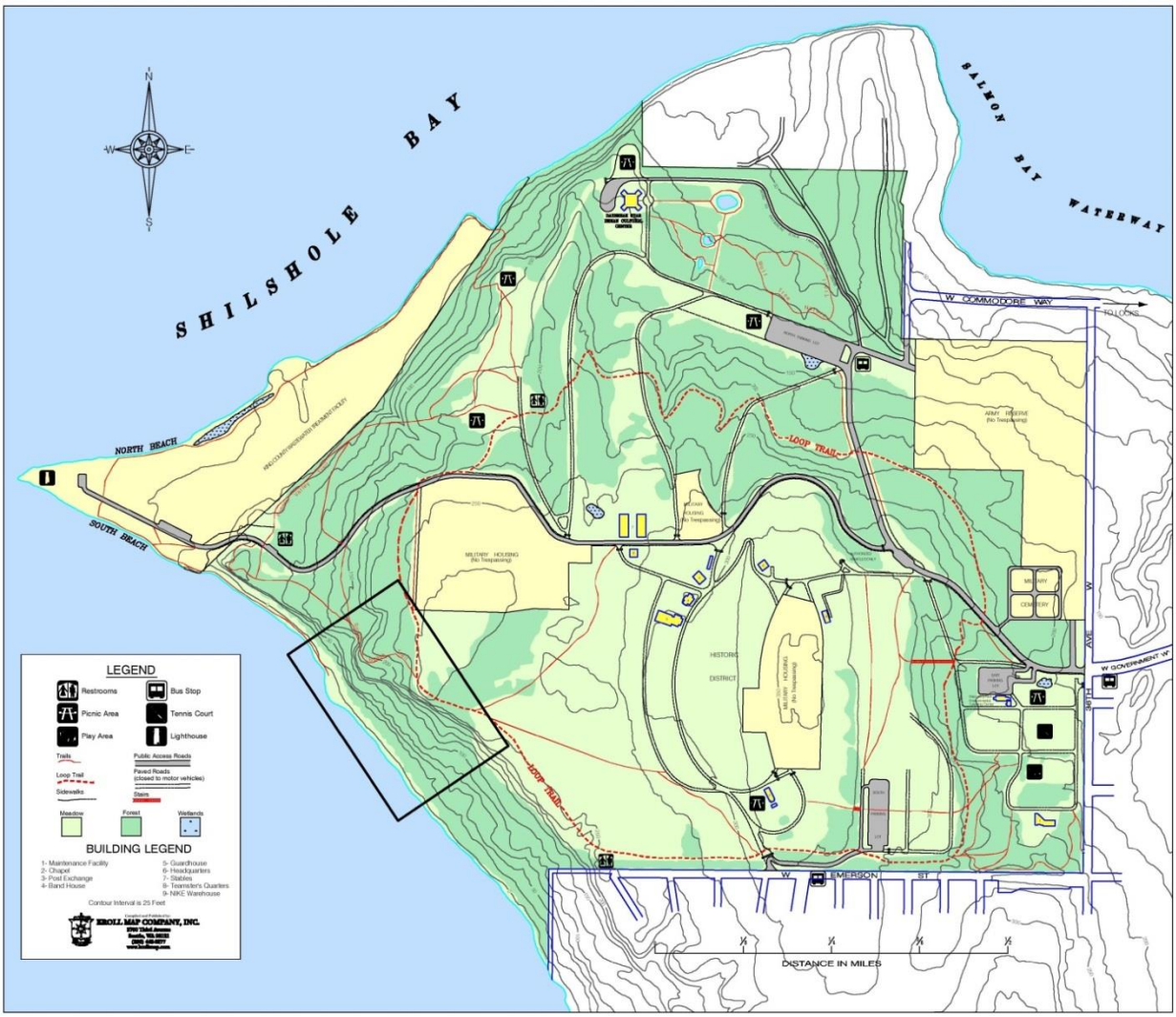

Figure 2: Map of Discovery Park, showing approximate area of the South Beach Bluff marked out in the black rectangle (City of Seattle, 2015).

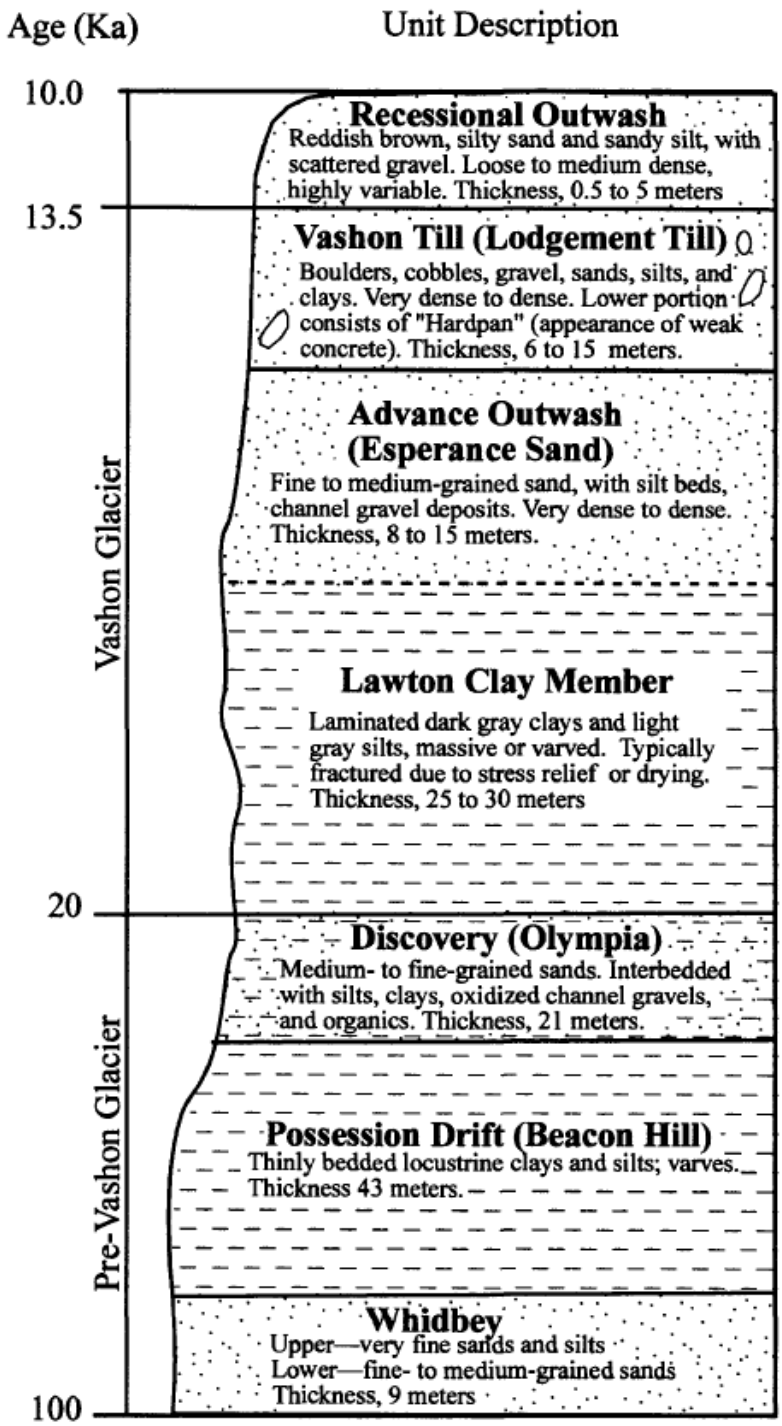

Figure 3: Generalized Quaternary sequence in the Puget Sound (Savage, 2000, from Galster and Laprade, 1991).

Figure 4: Photo from 3/6/2015, marking out unit locations on the bluff.

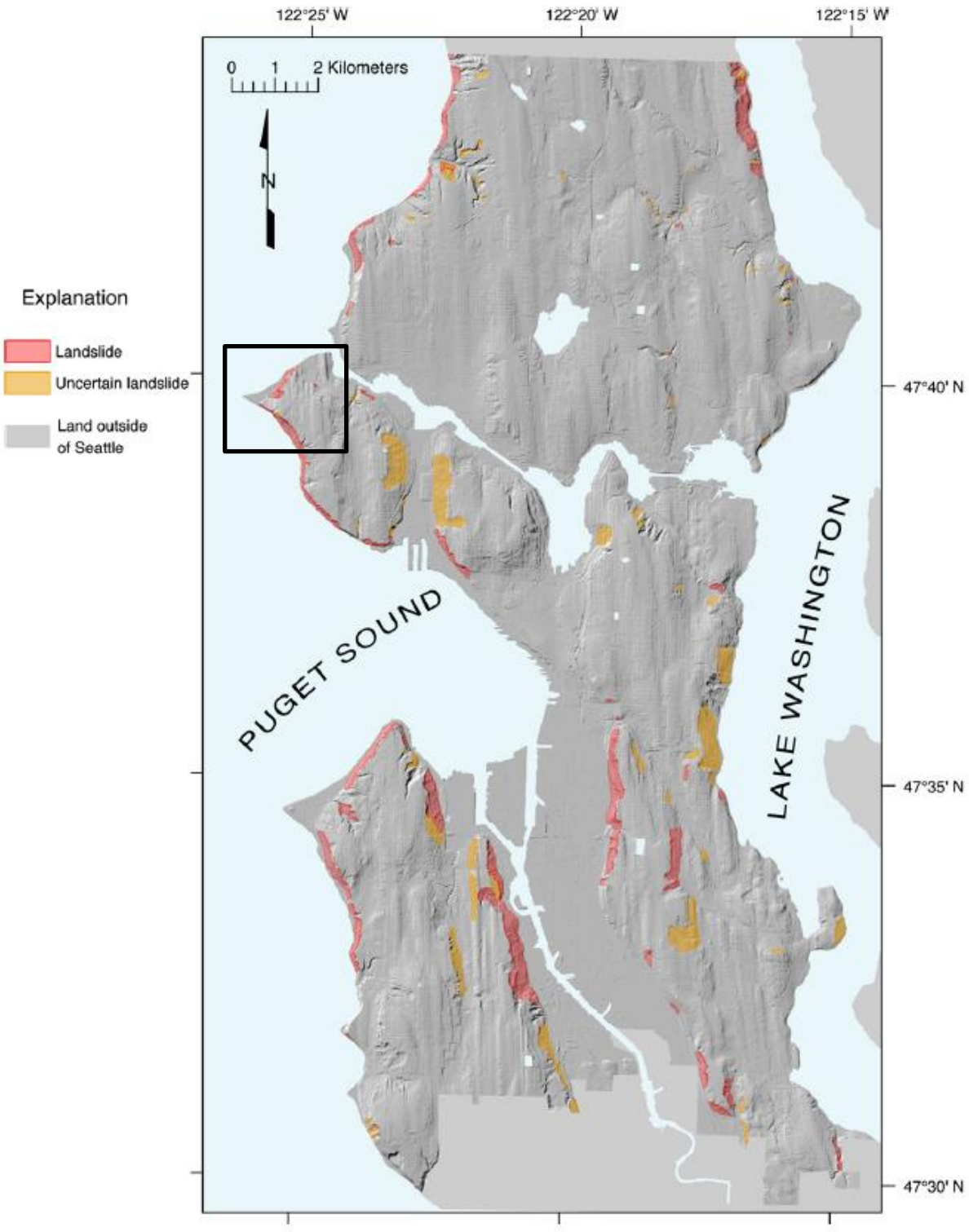

Figure 5: Landslides mapped using LiDAR on a shaded relief map generated from LiDAR-derived bare earth DEM (Schulz, 2007). Discovery Park is within the black rectangle.

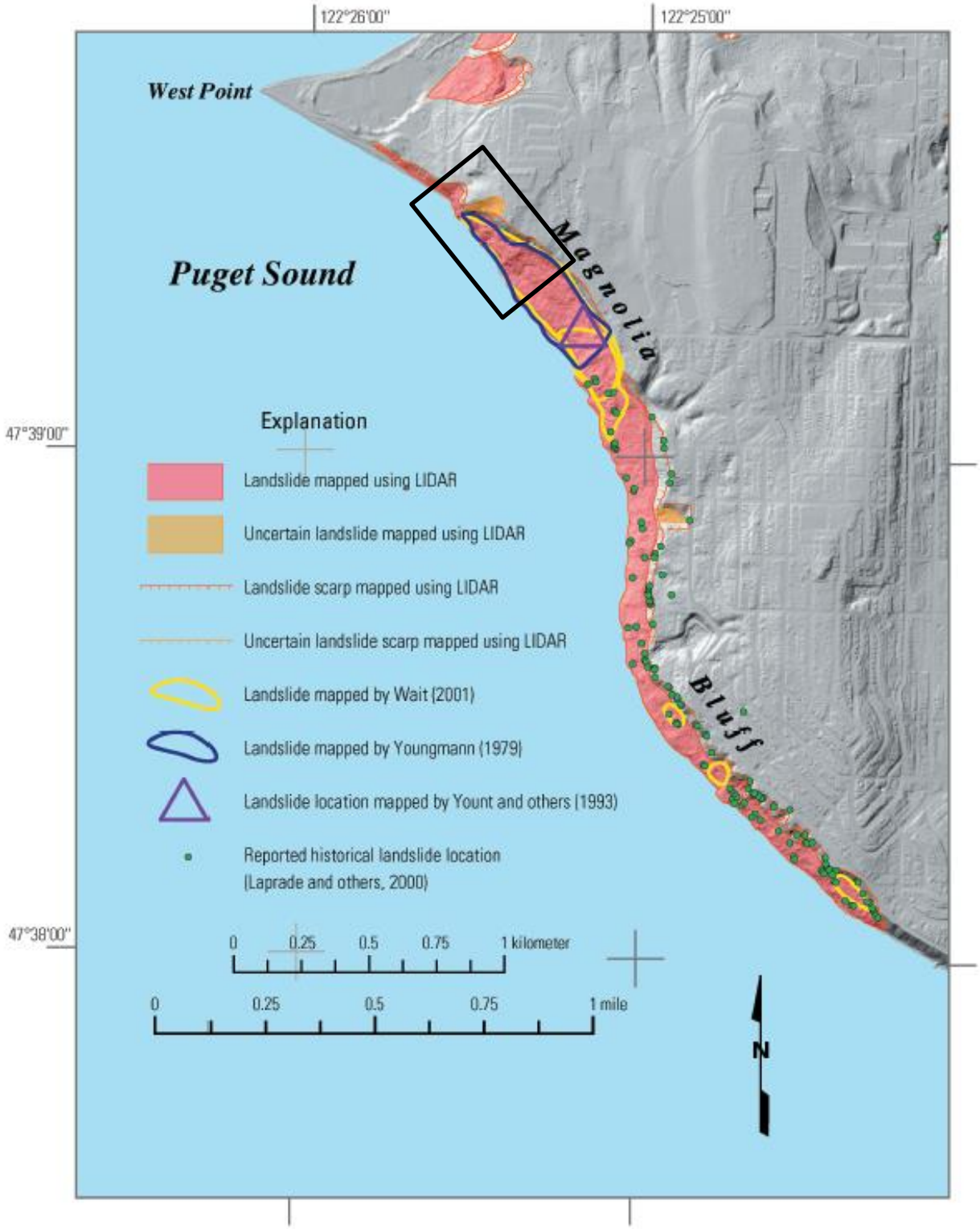

Figure 6: Landslides along Magnolia bluff mapped by hand and by LiDAR (Schulz, 2004). The South Beach Bluff is within the black rectangle.

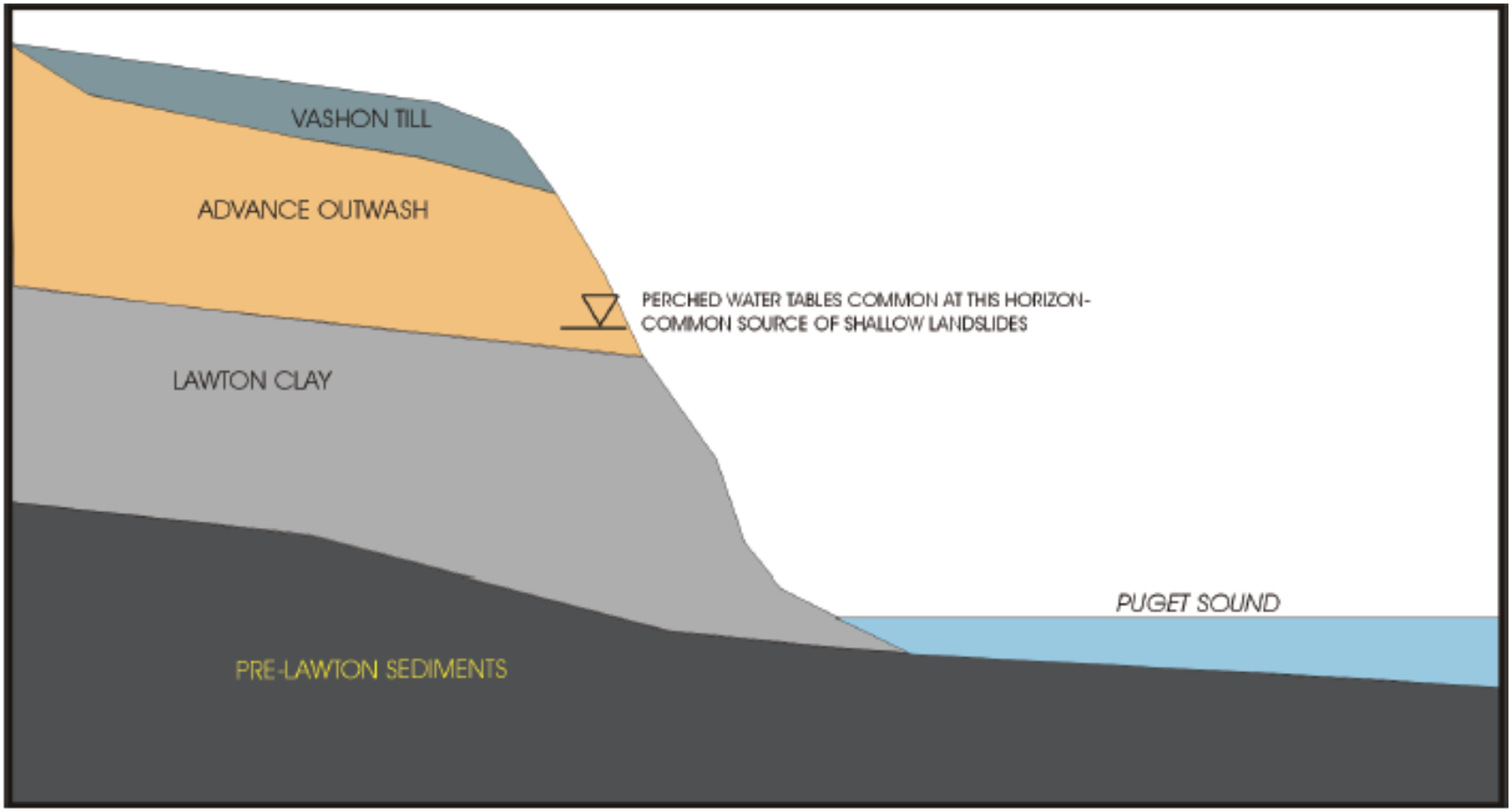

Figure 7: Stratigraphic sequence based off of Tubbs, 1974 (Harp et al., 2006)

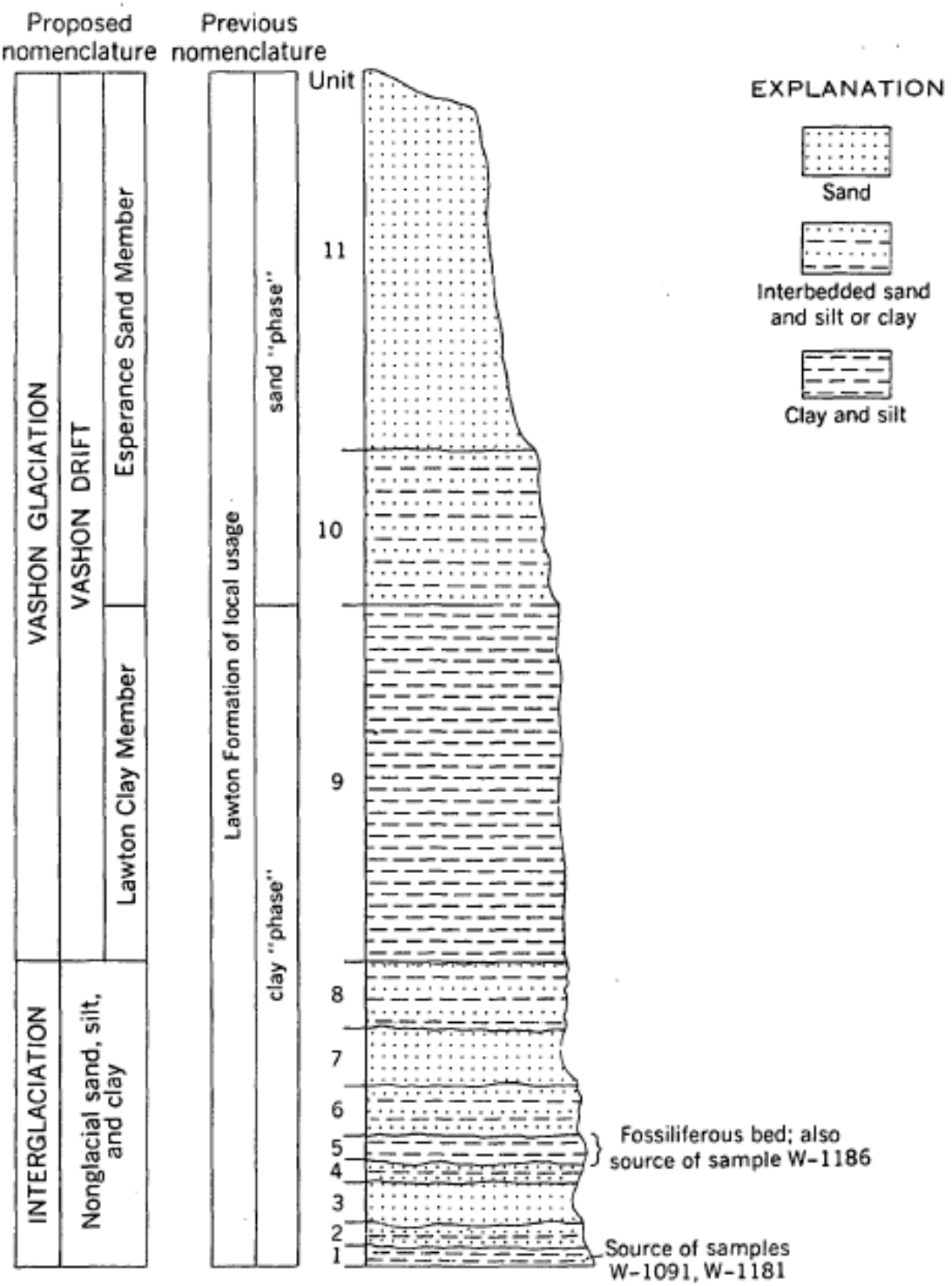

FIGURE 2.—Stratigraphy and subdivision of the nonglacial sediments and Vashon Drift exposed in sea cliff at Fort Lawton. (See measured section.)

Figure 8: Stratigraphic section at Discovery Park (Mullineaux et al., 1965)

Figure 9: Photos taken 5/17/2015, 11/21/2015, and 4/20/2016 respectively showing the change occurring over time at a distinctive fractured wedge at the northwestern corner of the bluff.

Figure 10: Site of sudden sheet failure witnessed by me and Dr. Juliet Crider, taken 4/8/2016.

Figure 11a (upper left): inaccessible joints marked out in red at the southeastern end of the study area.
Figure 11b (upper right): a joint set marked out in red and oriented parallel to the local bluff face at the northwestern end of the study area.
Figure 11c (lower left): red-black surface staining on joint surfaces.
Figure 11d (lower right): root infilling at the far southeastern forested end of the study area.

Figure 12: Beach view of bluff, with red line marking approximate path of tape measure, from 0m to 182.88m.

Figure 13: Beach view of bluff, with black arrows and lines marking northwest and southeast boundaries of the bluff focused upon for drone photography.

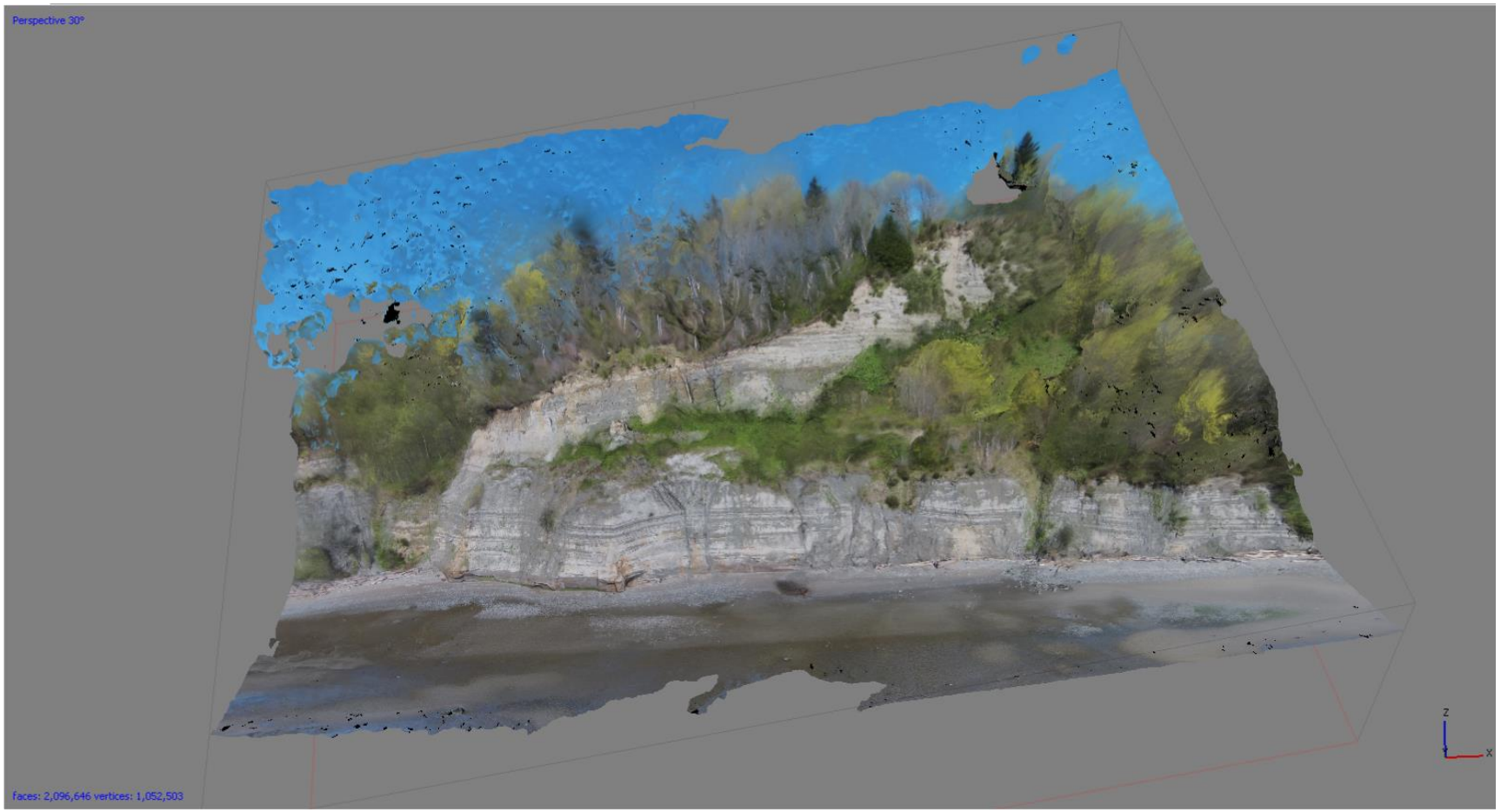

Figure 14: Completed SfM model, beach view.

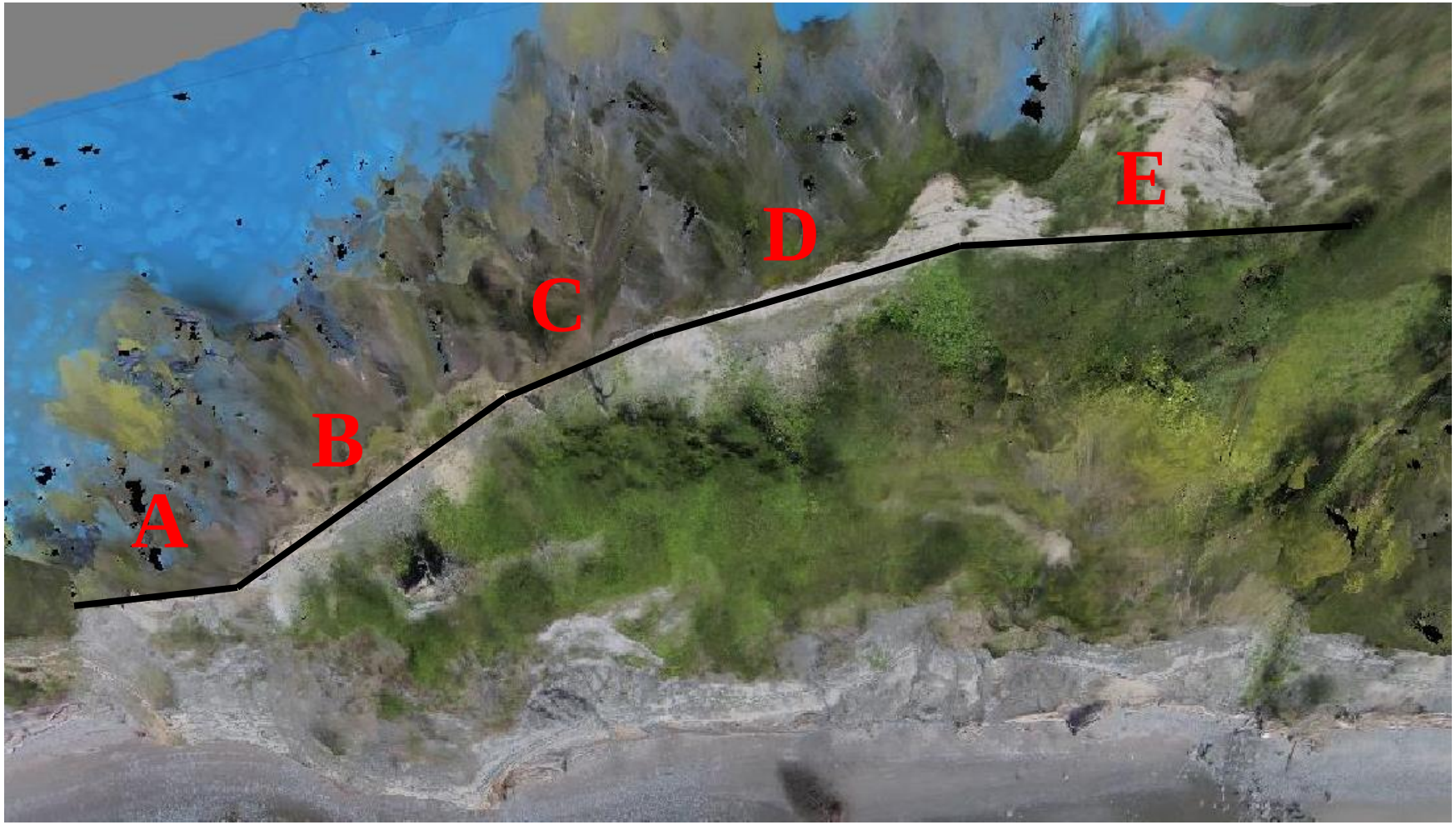

Figure 15: Oblique view of SfM model marked with domains.

Figure 16: Radial plumose surface texture and concentric arrest marks in the clay, marked with red arrows that indicate the directions of fracture development out from a (or several) point(s) of origin.

Figure 17: Ripples present in clay bedding.

Figure 18: Stair-stepping series of fractures marked out in red.

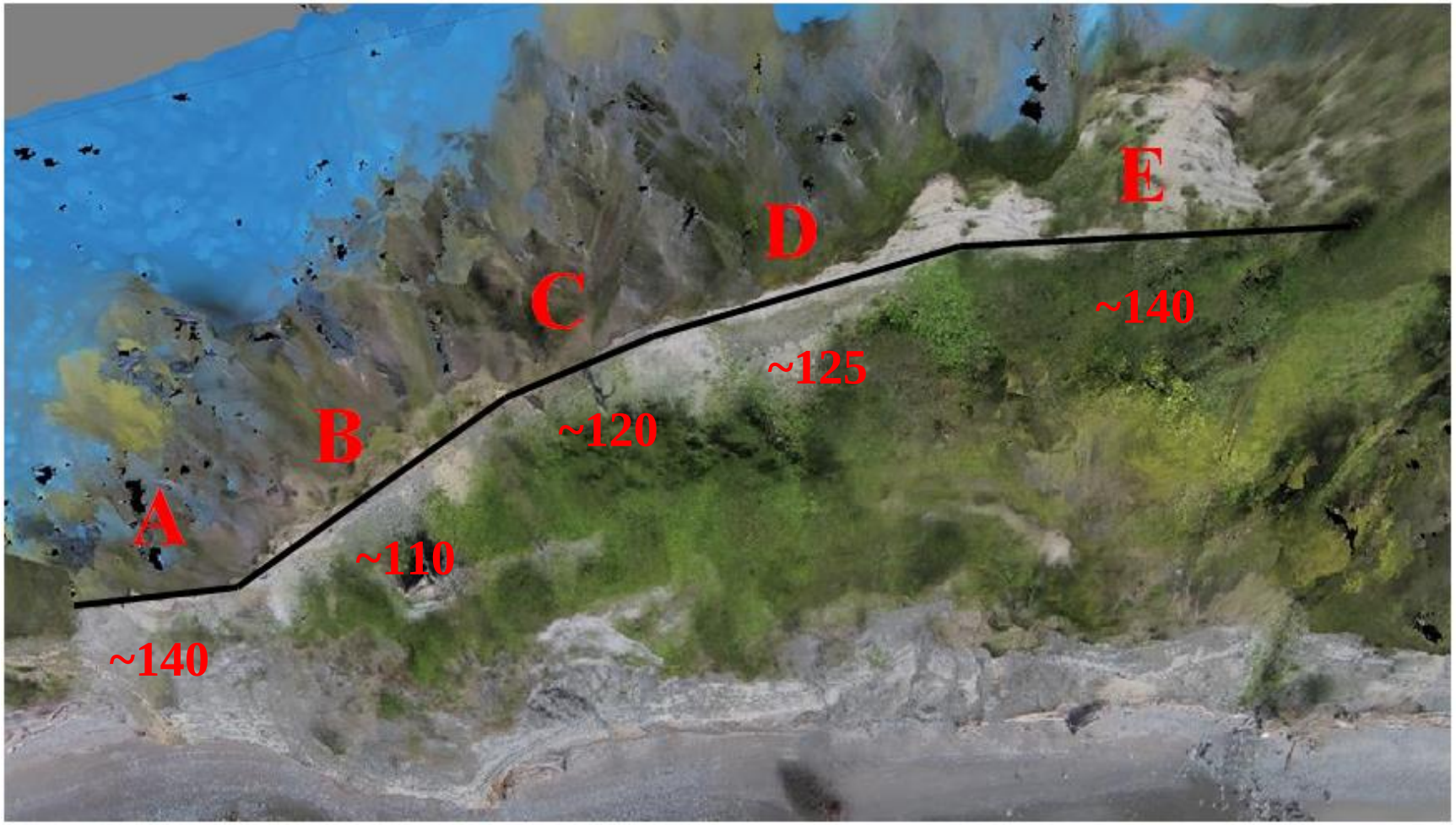

Figure 19: Oblique view of SfM model showing corresponding bluff angles at marked domains.

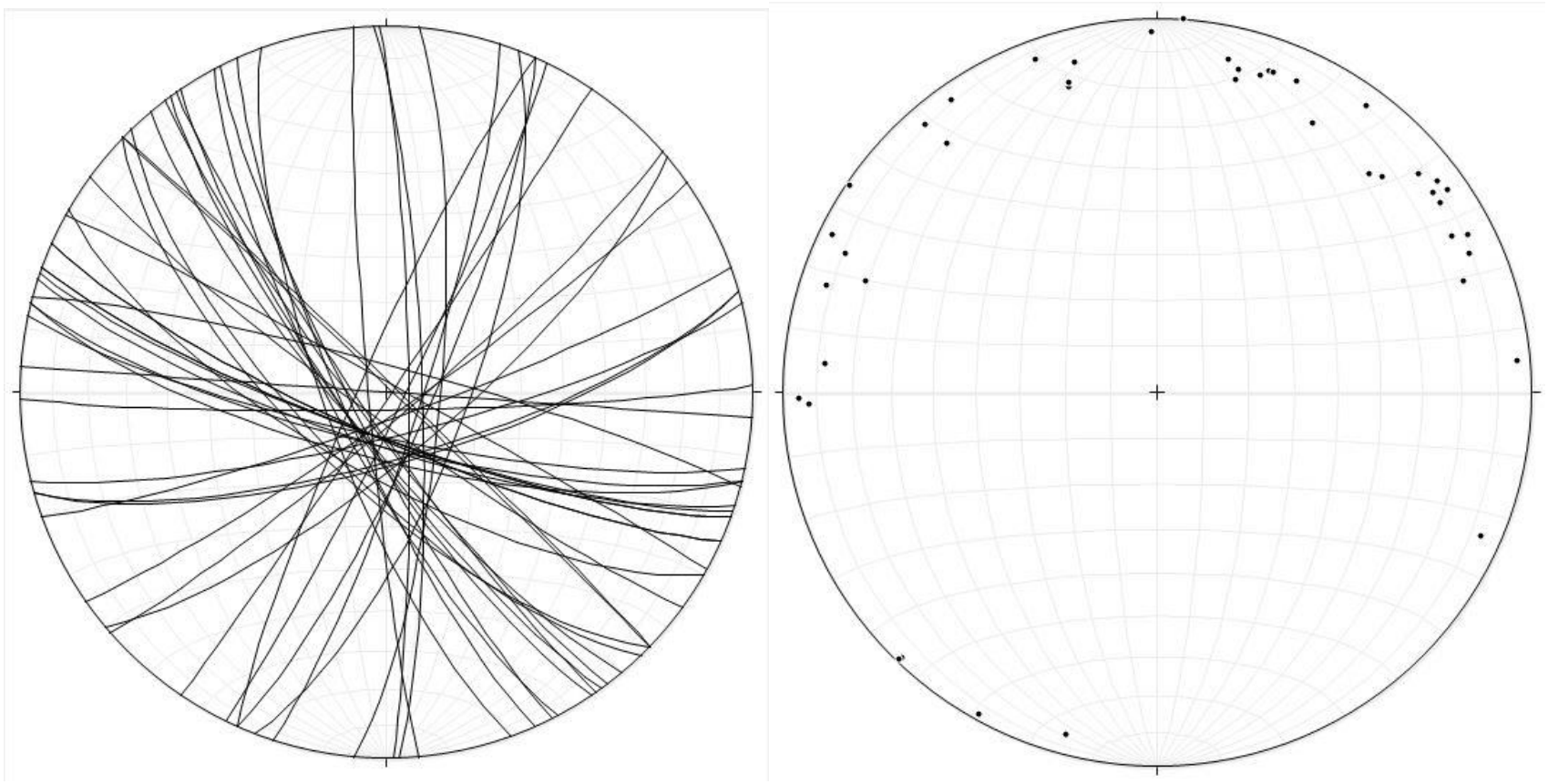

Figure 20a (left): Stereonet plot showing planes for all 45 joints measured.
Figure 20b (right): Stereonet plot showing poles to the measured joint planes.

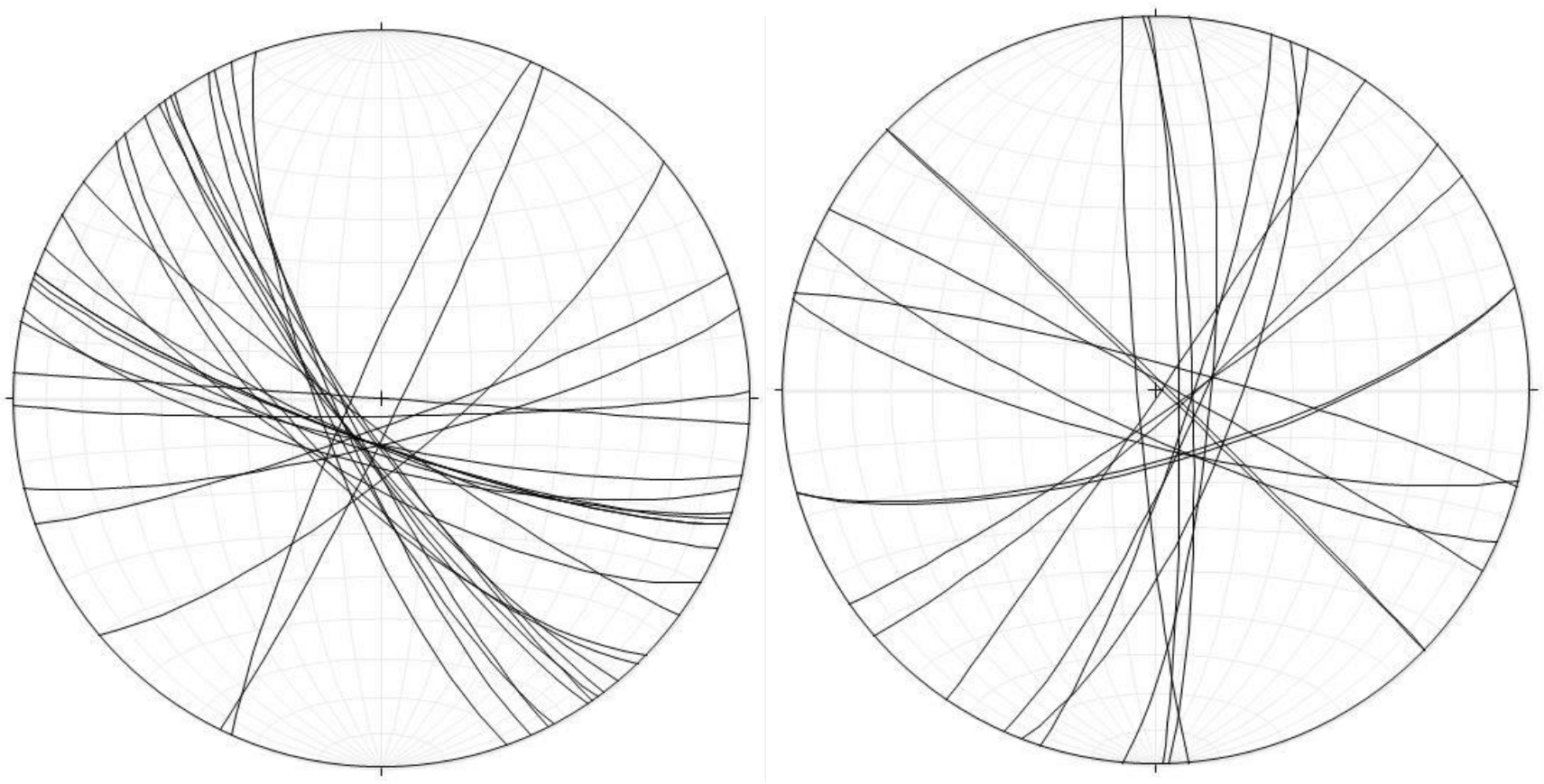

Figure 21a (left): Stereonet plot showing only that appeared in the field to be parallel to the local bluff orientation.
Figure 21b (right): Stereonet plot showing only joints that appeared in the field to be perpendicular to the local bluff orientation.

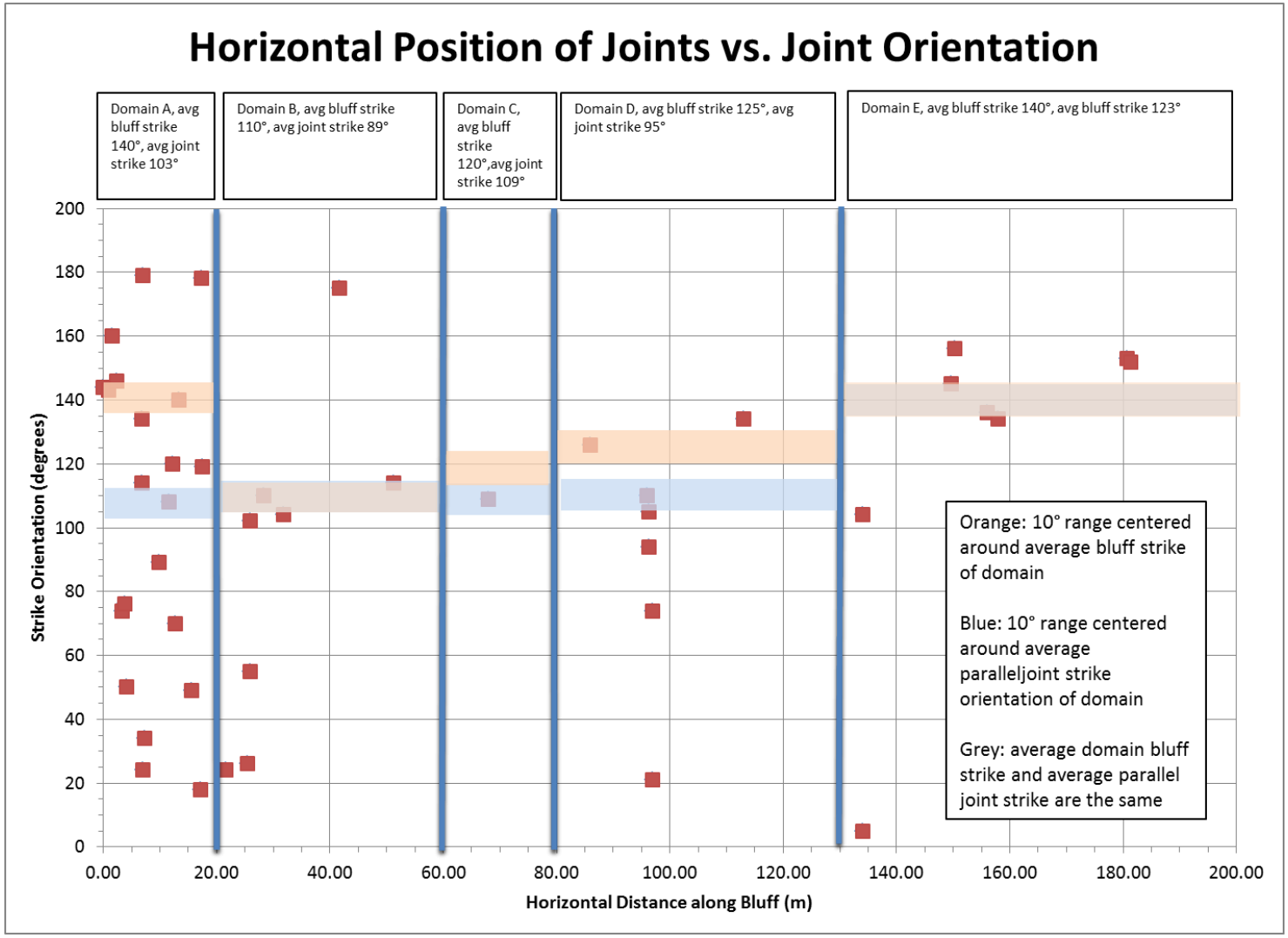

Figure 22: Scatterplot of joints plotted vs. horizontal location, showing joint orientation, the 5 domains, and the 10° range for bluff strike (orange) and parallel joint strike (blue) per domain, centered at the average. Domains B and E had the same average strike for bluff and parallel joint orientation, and overlap as a greyish band.

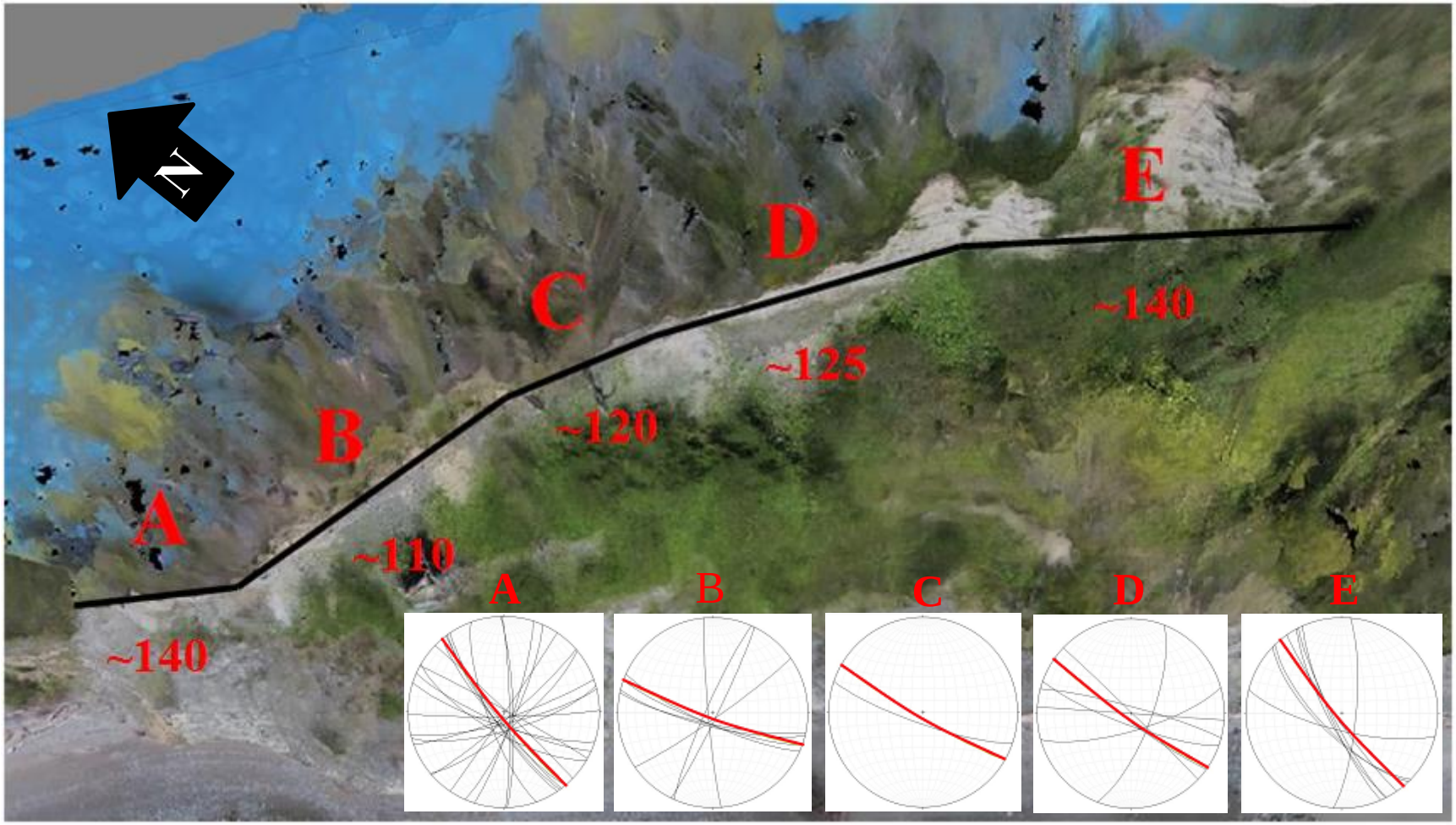

Figure 23: Oblique view of SfM model marked with domains, domain orientations, and stereonets containing joints measured within that domain, with a yellow-highlighted joint corresponding to the strike of the domain and to the average dip of 85°.

7.0 REFERENCES

Agisoft (2016) Help: PhotoScan Pro (v1.2.3): a Structure from Motion modeling program.

Allstadt, K. and Vidale, J. (2012) Seismically Induced Landsliding in Seattle: A Magnitude 7 Seattle Fault Earthquake Scenario. USGS NEHRP Final Technical Report, Grant Award Number G11AP20012. <http://earthquake.usgs.gov/research/external/reports/G11AP20012.pdf>

Allmendinger, R.W. (2016) Stereonet 9, <http://www.geo.cornell.edu/geology/faculty/RWA/programs/stereonet.html> (accessed April 2016)

Allmendinger, R.W., Cardozo, N.C., and Fisher, D. (2013) Structural Geology Algorithms: Vectors & Tensors: Cambridge, England, Cambridge University Press, 289 pp.

Augustinus, P.C., and Selby, M.J. (1990) Rock slope development in McMurdo Oasis, Antarctica, and implications for interpretations of glacial history, Geogprafiska Annaler, 72A, 55 – 62pp.

Booth, D.K., Troost, K.G., and Hagstrum, J.T. (2004) Deformation of Quaternary strata and its relationship to crustal folds and faults, south-central Puget Lowland, Washington State. Geology, vol. 32, p. 505-508

Borden, R.K. and Troost, K.G. (2001) Late Pleistocene stratigraphy in the South-Central Puget Lowland, West-Central Pierce County, Washington. Washington Division of Geology and Earth Resources Report of Investigations 33, 34 p

ten Brink, U.S., Molzer, P.C., Fisher, M.A., Blakely, R.J., Bucknam, R.C., Parsons, T., Crosson, R.S., and Creager, K.C. (2002) Subsurface Geometry and Evolution of the Seattle Fault Zone and the Seattle Basin, Washington. Bulletin of the Seimological Society of America, vol. 92, no. 5, p. 1737-1753

Cardozo, N.C. and Allmendinger, R.W. (2013) Spherical projections with OSXStereonet: Computers & Geosciences, v. 51, no. 0, p. 193 - 205, doi: 10.1016/j.cageo.2012.07.021

City of Seattle. (2007) Discovery Park History: Fort Lawton. Seattle Parks and Recreation. <http://www.seattle.gov/parks/parkspaces/discoverypark/history.htm> (accessed April 2016)

City of Seattle. (2015) Discovery Park Trails. Seattle Parks and Recreation. <http://www.seattle.gov/parks/trails_detail.asp?id=310> (accessed April 2016)

DJI (2015) Phantom 2 Vision+ User Manual v.1.8 (English): <http://dl.djicdn.com/downloads/phantom_2_vision_plus/en/Phantom_2_Vision_Plus_User_Manual_v1.8_en.pdf>

Galster, R.W., and Laprade, W.T. (1991) Geology of Seattle, Washington, United States of America: Bulletin of the Association of Engineering Geologists, v. 28, no. 3, p.235-302.

Goehring, L. (2013) Evolving fracture patterns: columnar joints, mud cracks and polygonal terrain. Philosophical Transactions of The Royal Society, 371: 20120353. <http://dx.doi.org/10.1098/rsta.2012.0353>

Harp, E.L., Michael, J.A., and Laprade, W.T. (2006) Shallow-Landslide Hazard Map of Seattle, Washington. U. S. Geological Survey Open-File Report 2006-1139

Hegelson, D.E. and Aydin, A. (1991) Characteristics of joint propagation across layer interfaces in sedimentary rocks. Journal of Structural Geology, vol. 13, no. 8, p. 897 – 911.

Hencher, S. (2012) Practical Engineering Geology. Abington, Spon Press, 450p.

mmattix-esristaff. (2012) <https://geonet.esri.com/thread/45105> (accessed April 2016)

Mullineaux, D.R., Waldron, H.H., and Rubin, M. (1965) Stratigraphy and Chronology of Late Interglacial and Early Vashon Glacial Time in the Seattle Area, Washington, U.S. Geological Survey Bulletin 1194-0, 10p.

Narr, W. and Suppe, J. (1991) Joint spacing in sedimentary rocks. Journal of Structural Geology, vol. 11, no. 9, p. 1037 – 1048.

Niethammer, U., James, M.R., Rothmund, S., Travelletti, J., Joswig, W. (2012) UAV-based remote sensing of the Super Sauze landslide: evaluation and results: Engineering Geology, v. 128, no. 1, p. 2-11.

Porter, S.C. and Swanson, T.W. (1998) Radiocarbon age constraints on rates of advance and retreat of the Puget Lobe of the Cordilleran Ice Sheet during the last glaciation: Quaternary Research, v. 50, p. 205-213, doi: 10.1006/qres.1998.2004.

Russell, T.S. (2016) Calculating the Uncertainty of a Structure from Motion (SfM) Model, Cadman Quarry, Monroe, Washington, University of Washington, MESSAGe Technical Report Number: 30, 39p.

Savage, W.Z., Morrissey, M.M., and Baum, R.L. (2000) Geotechnical properties for landslide-prone Seattle-area glacial deposits. U.S. Geological Survey Open-File Report 2000-228

Selby, M.J. (1993) Hillslope Materials and Processes: 2nd edition. Oxford, Oxford University Press, 451p.

Schulz, W.H. (2004) Landslides mapped using LiDAR imagery, Seattle, Washington. U.S. Geological Survey Open-File Report 2004-1396

Schulz, W.H. (2005) Landslide Susceptibility Estimated From Mapping Using Light Detection and Ranging (LIDAR) Imagery and Historical Landslide Records, Seattle, Washington. U.S. Geological Survey Open-File Report 2005-1405

Schulz, W.H. (2007) Landslide susceptibility revealed by LIDAR imagery and historical records, Seattle, Washington. Engineering Geology, Volume 89, Issues 1–2, 12 January 2007, Pages 67-87.

Shannon & Wilson, Inc. (2000) Seattle Landslide Study, Geotechnical Report Vol. 1, for Seattle Public Utilities, Seattle, Washington, 225p.

Shipman, H. (2001) Coastal Landsliding on Puget Sound: A review of landslides occurring between 1996 and 1999. Washington State Department of Ecology, Report #01-06-019

Shipman, H. (2004) Coastal Bluffs and Sea Cliffs on Puget Sound, Washington. U. S. Geological Survey Professional Paper 1693, pp. 81-95

Stephenson, D.A., Fleming, A.H., and Mickelson, D.M. (1988) Glacial Deposits, *in* Back, W., Rosenshein, J.S., and Seaber, P.R., eds., Hydrogeology: Boulder, Colorado, Geological Society of America, The Geology of North America, v. 0~2.

Thorson, R.M. (1979) Ice-Sheet Glaciation of the Puget Lowland, Washington, during the Vashon Stade (Late Pleistocene). Quaternary Research, vol. 13, p. 303-321

Trimble. (2015) Trimble Geo 7x Datasheet: <http://trl.trimble.com/docushare/dsweb/Get/Document-730024/022516-098A_Geo%207Xw%20Access_DS_US_0415_LR.pdf> (accessed April 2016)

Troost, K.G. and Booth, D.B. (2008) Geology of Seattle and the Seattle area. Washington. Geological Society of America Reviews in Engineering Geology, vol. 20. p. 1-35

Tubbs, D.W. (1974) Landslides in Seattle: Washington Division of Geology and Earth Resources Information Circular 52, Olympia, Washington, Washington Division

Tubbs, D.W. (1975) Causes, Mechanisms, and Prediction of Landsliding in Seattle, University of Washington, PhD Dissertation, 67p.

Tubbs, D.W, and Dunne, T. (1977) Geologic Hazards in Seattle, A field guide for The Geological Society of America Annual Meeting, 28p.

Wells, R.E., Weaver, C.S., and Blakely, R.J. (1998) Fore-arc migration in Cascadia and its neotectonic significance. Geology, vol. 26, no. 8, p. 759 – 76

8.0 APPENDICES

GPS CONTROL POINTS:

NOTES ON GPS AND SfM PROCESSING:

The data stored on the Trimble Geo7x unit can be transferred to a workable ArcGIS format via the GPS Pathfinder Office program, located on select computers within Johnson Hall at the University of Washington. I attempted to transfer my two files but encountered difficulties with both computers available for graduate student use. I managed to successfully transfer the files onto the computer through the use of the GPS Pathfinder Office program installed on Kathy Troost's personal computer, but attempted to proceed with the differential processing with another computer.

Tait Russell, via personal correspondence, recommended the use of the Washington State Reference Network (WSRN) for downloading the appropriate correction files, instead of performing the differential processing through GPS Pathfinder Office. However, the correction files could only be downloaded in brackets of time no greater than 99 hours and 99 minutes. Because one of my files, the 9-point bench file, spanned from 2:30pm on April 1st to 5:20pm on April 6th, I couldn't download a correction file that covered the amount of time I needed to have differentially processed.

Returning to GPS Pathfinder Office produced a different error; before proceeding with the differential processing, the program stated: "Warning: One or more of the selected SSF file(s) are invalid or contain invalid time period information." Continuing with the differential processing resulted in a failed conversion error. Troubleshooting and searching for the problem resulted in an explanation found on the ESRI forums regarding errors that arose when collecting data in SSF files that remained open over consecutive days. The answer supplied by the ESRI staff member to a direct question about the exact same error code strongly suggested that one file be created per data collection period, closed at the termination of the session, and a brand new file created for the next day of data collection in order to avoid being unable to differentially process the data (mmattix-esristaff, 2012). Since my GPS file encompassed too broad of a timeframe, it was unworkable. Once I realized this error, two options were available: to either retake the all points entirely, or to find a way to subdivide the data file into three separate files that comprised the shorter timeframes in which I had taken data for each day. Referencing the Agisoft SfM model again gave me reason to reconsider the feasibility of applying accurate GPS points to the model, and with consultation from Tait Russell and my advisors, I decided against attempting to georeference the model.

The SfM model itself was not ideal. The DJI Phantom 2 Vision+ drone has no water resistance and cannot operate in rain, snow, or fog, in addition to conditions of strong wind and sub-freezing temperatures (DJI, 2015). Although conditions during the photo collection were sufficient to fly the UAV, continuous rain over the warm 2015 – 2016 winter resulted in unusually dense springtime vegetation. Structure from Motion relies entirely on photography, meaning that high visibility is paramount. There needs to be clear exposures of the surfaces to be modeled, in addition to a reliable, stable light source to allow the modeling program to properly correlate the patterns present in the pictures and generate a 3-dimensional surface. Bare bluff surfaces were well-modeled and clear, but this vegetation obscured the majority of the bench surface and the modeling resulted in a mostly-indistinct green mass in several key areas. The upper tree line was similarly affected; this error results from the inability of the program to accurately distinguish between separate plants due to the pattern similarity in color and structure. A close-up view of these blurry portions is located further down in the appendix together with the additional SfM views. The indistinct modeling of the bluff in these areas made it difficult to pinpoint the 12 locations where I took GPS points to georeference the model. Only a few of the 9 points at the bench level and none of the 3 points at the base of the upper tree line could be clearly identified in the model due to both the vegetation and the resolution. As powerful as it was, the computer used to process the photos used for SfM did not have the computing power to generate a model to finer detail under the parameters provided.

TABLE 1: JOINT ORIENTATIONS AND HORIZONTAL LOCATIONS

Joint #	Location (decimal ft)	Location (m)	Strike	Dip	Orientation*
1	0	0	144	80	parallel
2	2.8	0.85	143	83	parallel
3	5	1.52	160	76	parallel
4	7.9	2.41	146	80	parallel
5	11.1	3.38	74	74	perpendicular
6	12.6	3.84	76	80	parallel
7	13.7	4.18	50	76	parallel
8	22.3	6.80	314	88	perpendicular
9	22.4	6.83	114	80	parallel
10	22.7	6.92	24	80	perpendicular
11	22.7	6.92	359	85	perpendicular
12	24.1	7.35	34	89	perpendicular
13	32.3	9.85	89	86	parallel
14	38.2	11.64	108	78	parallel
15	40.1	12.22	120	72	parallel
16	41.9	12.77	70	84	parallel
17	44	13.41	140	80	parallel
18	51.3	15.64	49	84	perpendicular
19	56.5	17.22	18	82	perpendicular
20	56.8	17.31	358	82	perpendicular
21	57.1	17.40	299	88	perpendicular
22	71	21.64	204	84	parallel
23	83.4	25.42	26	86	parallel
24	85	25.91	102	80	parallel
25	85	25.91	55	85	perpendicular
26	92.7	28.25	110	80	parallel
27	104.5	31.85	104	78	perpendicular
28	137	41.76	175	86	perpendicular
29	168	51.21	114	80	perpendicular
30	223	67.97	109	80	parallel
31	282	85.95	126	84	parallel
32	315	96.01	110	80	parallel
33	316	96.32	285	84	perpendicular
34	316.2	96.38	94	90	parallel
35	317.8	96.87	74	75	perpendicular
36	318.1	96.96	21	72	perpendicular
37	371	113.08	314	89	perpendicular
38	440	134.11	104	75	parallel
39	440	134.11	5	78	perpendicular

40	490.9	149.63	145	84	parallel
41	493.3	150.36	156	80	parallel
42	512	156.06	136	72	parallel
43	518	157.89	134	70	parallel
44	593	180.75	153	82	parallel
45	595	181.36	152	78	parallel

*The determination of joints as parallel or perpendicular to the bluff was relative to the local, immediate block at which the joint was measured.

DETAILED FIELD NOTES:

Table 1above lists the joints measured. The joints could be split into two main patterns: failure planes roughly parallel to the face of the bluff, and failure planes perpendicular to or intersecting the face of the bluff. Parallel and perpendicular joints are differentiated in Table 1 in a separate column. Strikes and dips were measured according to the "right hand rule": a flat, extended right hand is oriented parallel to the plane measured, with the fingers pointing in the direction of downward dip. The direction of the thumb then indicates the strike orientation.

Observations of the bluff were taken along the length of an inch-feet and decimal-feet tape measure; the horizontal distance of the bluff was long enough that the tape had to be moved several times and the distance recalculated. These horizontal values were converted to meters for Table 1 and the following observations. The starting and end points of the tape are marked on Figure 12.

From 0 – 2.4m, the strike of the bluff was roughly estimated to be 144 degrees. This area primarily went across a series of sheets with fractures approximately parallel to the corner, spaced about 10cm – 1m apart. There was no distinct chemical or detrital infilling, although the surface was dusty from powdered material from higher on the bluff, and some exposed joint surfaces showed a reddish, dark brown and black discoloration that may have been indicative of past water movement; some joints were separated by some root material and insects activity. Most of lower exposure was covered in clay talus; very dry, tan/grey in color, and powdery in texture. Failure modes observed at this location were either in small blocks or wedges.

From 0 – 5.2m, outside of major, easily accessible joint surfaces, most of the exposure was highly fractured and irregular, with minor apertures of 0.1 – 0.5mm and spacing of 1-20cm in irregular directions. The fresh surfaces were dark grey, and fractured blocks were easily dislodged out of the surface by hand. Some of the blocks pulled out of the surface left behind rounded, concretion-shaped holes to match the shape of the block. With the exception of those rounded edges, upper bluff failure at this zone tended to happen along the horizontal bedding planes present in the clay itself and the major perpendicular and parallel joint planes. Figure 16 shows a hand sample that was taken from one of these rounded blocks; the ISRM description of the material is as follows: This sample is S6 grade (very hard) clay, indented with difficulty by a thumbnail. It could also be described as weak rock; the clay is very difficult to penetrate with a knife. Although it splits readily along bedding planes and fractures under light blows from a geological hammer, it cannot easily be shaved off with a sharp edge.

The fractures and failures in the talus and near-surface weathered portions closer to the bench level broke more irregularly than fractured portions that were set further back in the bluff that were darker in color and indicative of more moisture and less weathering. It appeared that these larger, more coherent portions failed in both smaller blocks and larger, massive sheets up to 2 – 3 meters square.

From 2.4 – 20.1m, the strike of the bluff was estimated to be roughly 130 degrees. This estimate was taken by standing parallel to a consistently-striking portion of the bluff, and orienting the compass using the right-hand rule. At 17m, the upper portion of bluff appeared to change strike while the lower portion of the bluff remained about 144 degrees; this was apparent from larger, inaccessible joints that split the talus cone and fractured blocky material from the remainder of the bluff.

20.1m onwards marked a change in bluff strike to be more directly south-facing, about 115 degrees. At 20.1m, a large corner wedge was visibly separated from the upper portion of bluff, which was set further back by 1 – 3m. The upper bluff seemed to fail differently than the lower bluff closer to the bench, even though this exposed corner of the bluff as a whole has little obstructive vegetation and is exposed to the

same amount of weathering. From bench-level, the upper half appeared primarily intact, with very minor perpendicular fractures that were often covered in soil wash and organic debris from above. Most of the fractures appeared to be shallow and roughly parallel to the bluff face, with the apertures only discernable by the stairstepping pattern produced by sun shadow. Some wedge blocks above the talus slope exhibited very particular radial fractures, seen in Figure 16. The very dry, crumbled blocks fallen from above and lying at bench-level broke easily along the bedding in sheets, revealing the ripple structures in Figure 17.

At 26.2m, the upper bluff was marked by larger, thicker, longer sheet fractures with an irregular perpendicular fracture plane, a smooth horizontal upper plane that failed along the bedding, and a smooth fracture plane against the bluff surface.

From 27.4 – 62.5m was an area of apparently frequent collapse, displaying fresh blocks down on the bench level and fallen young trees from the top of the bluff. These trees had fallen very recently; the leaves were still green and growing, and the roots either exposed, clumped together with original soil material, or buried beneath a mixture of sand and clay. From 32 – 110.9m, the bluff material at the bench-material transitioned from the tan, crumbly dry material and more into dark grey, firm, wetter material that was more densely vegetated.

51.2m was at an older, seemingly more resistant portion of the bluff, covered in a significant amount of overhead dark soil wash and overgrown with lichen and moss. The resulting disintegrated soil mix on the surface of the talus cone made it ideal for insect burrows. Despite the evidence for large and recent collapses in this stretch of the bluff, it was difficult to verify visually joints present in the upper half of the bluff. The color of the clay underlying the soil material was dark, presumably indicating water seepage out from the upper contact of clay with sand, or water seepage out of sand lenses within the upper transitionary portion of the clay unit.

From 62.5 – 87.2m, the water flow over the bluff surface became evident; sheets of plant roots were growing on the surface, with plenty of moss, lichen, sprouting plants and horsetail. Although what few joints present available for measurement were difficult to see due to the amount of plant material, the exposed surfaces were dark and moist, often featuring a dense infilling of roots and moss. There were few prominent or pervasive joints due to both the visually coherency of the bluff and due to the reattachment of fallen clay particles onto the lower surface, resulting in a dark, indistinct, nubby texture. The talus material beneath this zone was a dark clay partially covered in more vegetation and broken logs. The clay was broken up, but hardly powdery or sharp-edged like that from the northwestern corner of the bench where measurements started.

At 72.5m, the bluff strike transitioned again to about 130 degrees. At 75.3m, overhead seepage was observed coming out from the bluff at a fracture plane running parallel to the bluff face. About 10m above that point, there were fewer visible joints and the material was drier and more coherent. No seepage was observed, but vegetated surface coverage remained.

At 81.7m was an exposed, dark grey portion of bluff that was missing surface vegetation; I observed a large sheet failure at this location with my project advisor, Juliet Crider, on April 8st. This failure zone is featured in Figure 23. The exposed material was very moist and dark in color, possibly due to either moisture content or fresh exposure. The remainder of the 62.5 – 87.2m area appeared to be coherent, but this could have been an illusion brought upon by soil cover and vegetation growth obscuring underlying joints and prior fracture planes. At 85.3m was the stair-stepping end of this recent failure, showing evidence for irregular, long perpendicular failures and multiple layers of preexisting parallel joints. This is marked in Figure 18.

At 87.2m was the corner edge of another large failure, differentiated from the others closer to the northwestern end of the bluff by the appearance of sand in the talus material directly underneath. The apparent dryness of the upper bluff could possibly have been due to the presence of sand covering the face. However, like with the remainder of the bluff within this area, it was difficult to pick out joints in the lower exposures of clay due to bumpy reattachment surfaces.

At 101.5m, the bluff transitioned back to an overall damp clay covered in vegetation with a drier, coherent upper unit. Enough seepage was present at this location to support the dense growth of horsetail out of the surface. At this location, the only lower visible failures appeared to be small sloughing movements of the clayey talus material away from the main bluff face. At 103.6m, the presence of sandy transition lenses in the uppermost section of the clay unit underneath the sand unit become evident; the density of insect burrows in the sand lenses indicate a change in material significant enough to be distinguished from the remainder.

110.9m marked the point where medium quartz sand became the primary talus material on the bench due a combination of increasing vertical thicknesses of the uppermost overlying sand unit, increasing frequency of sand lenses at the transition zone between the clay and the sand, and decreasing vertical thicknesses of lower exposures of the underlying clay unit. The actual thickness of the clay was unlikely to have changed; however, the greater size of the sandy talus cones moving further down the horizontal distance of the tape measure covered up more of the clay unit and exposed less of it to see.

At 116.7m was the beginning of a steep, sandy talus slope that moved upwards over clay and into the forested area off of main bluff. At 118.9m, visible seepage was again present at the top of the primary clary unit beneath a cap of sandy soil and grass.

At 134.1m was close to the top of the sandy talus pile, marked by a white log propped against the face of the bluff. Here, the approximate strike of the bluff appears to change to be about 170 degrees. Although larger, measureable joints in the lower portion of the bluff were infrequent from 20.1 – 134.1m, there were joint sets present in the transitionary zone between the sand and clay. The joints exposed in this forested region extended through cross-bedded sands and laminar clay varve sequences.

From 146.3 – 182.88m was the last stretch of measured bluff, hidden beneath tree cover in an entirely forested, sheltered area. What joints were present appeared to be primarily parallel to the bluff, featuring some smaller, evenly-spaced, parallel irregular fractures exhibiting red-black surfaces indicative of past groundwater movement against those surfaces. At 169.5m, some flat concretions were observed in a clay lens. These were the only concretions visible. The end of the tape was unable to be clearly marked in the model screenshot featured in Figure 12. Vegetation prevented further movement along the talus slope, which entirely obscured the underlying clay at this area. However, plants and moss growing on the bluff surface appeared to root deeper than just the overlying soil layer; some of the joints that were parallel to the bluff exhibited roots growing through the cracks and forming enough space to between the parallel sheet and the bluff to form small caves.

General notes about the bluff at bench-level; the outermost portion of the bench, away from the talus-covered bluff face and directly against the edge of the bench, exhibited a hummocky topography that was mostly hidden by a dense patch of young alders, blackberry, and horsetail. The winding trail used to descend from the trailhead at the top of the bluff down to bench level passed by audibly trickling water and over older, rotting woody debris sunken into soft, wet mud that adjacent to visible standing water—a small pond was mostly obscured by surrounding vegetation, but was large enough to make a deep splashing sound when objects were thrown into the center. From beach-level, visible, steady water trickling can be observed pouring down over the lowermost Olympia beds and down onto the beach.

ADDITIONAL SfM VIEWS:

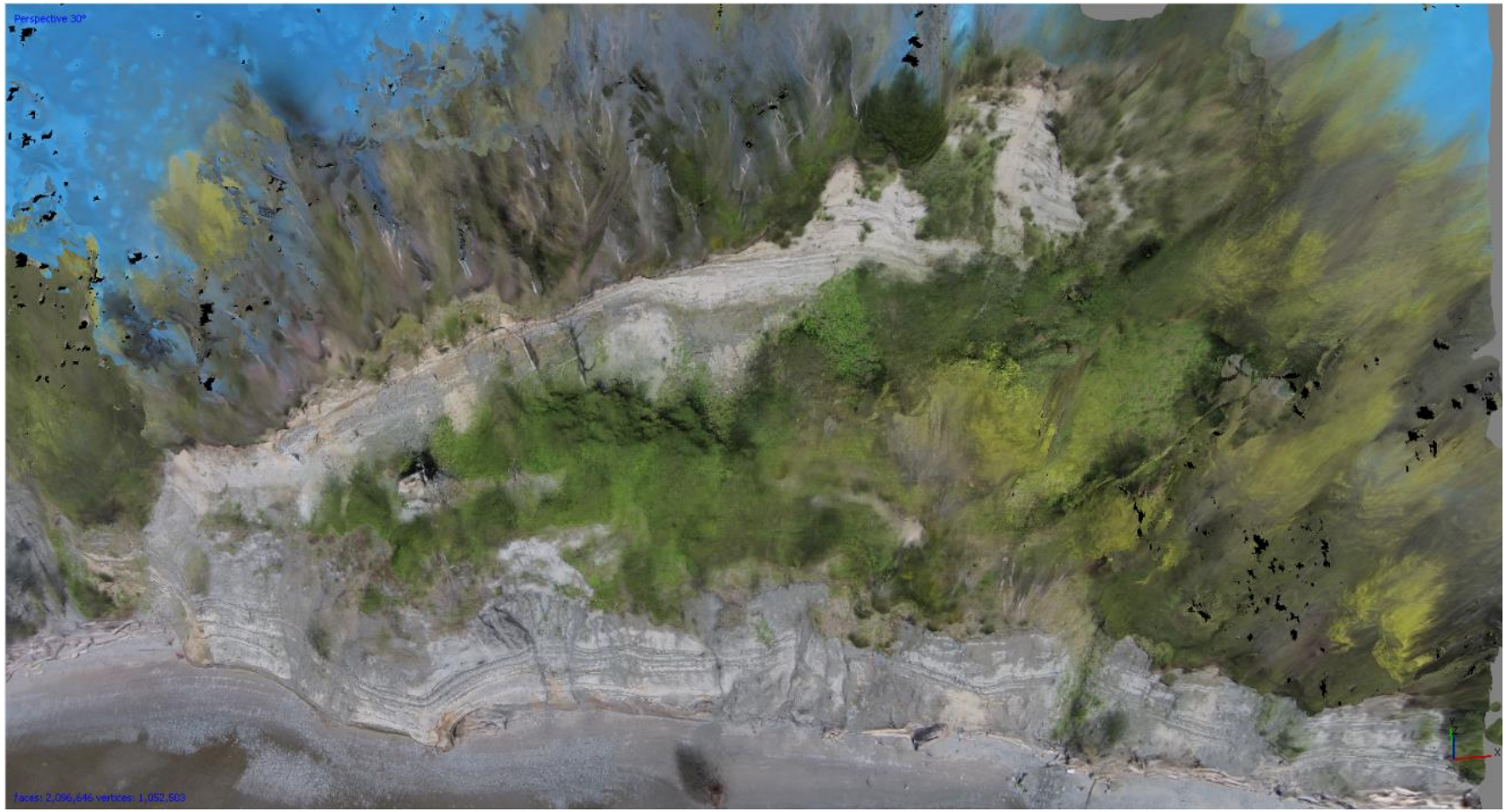

Angled bird’s-eye view of SfM model.

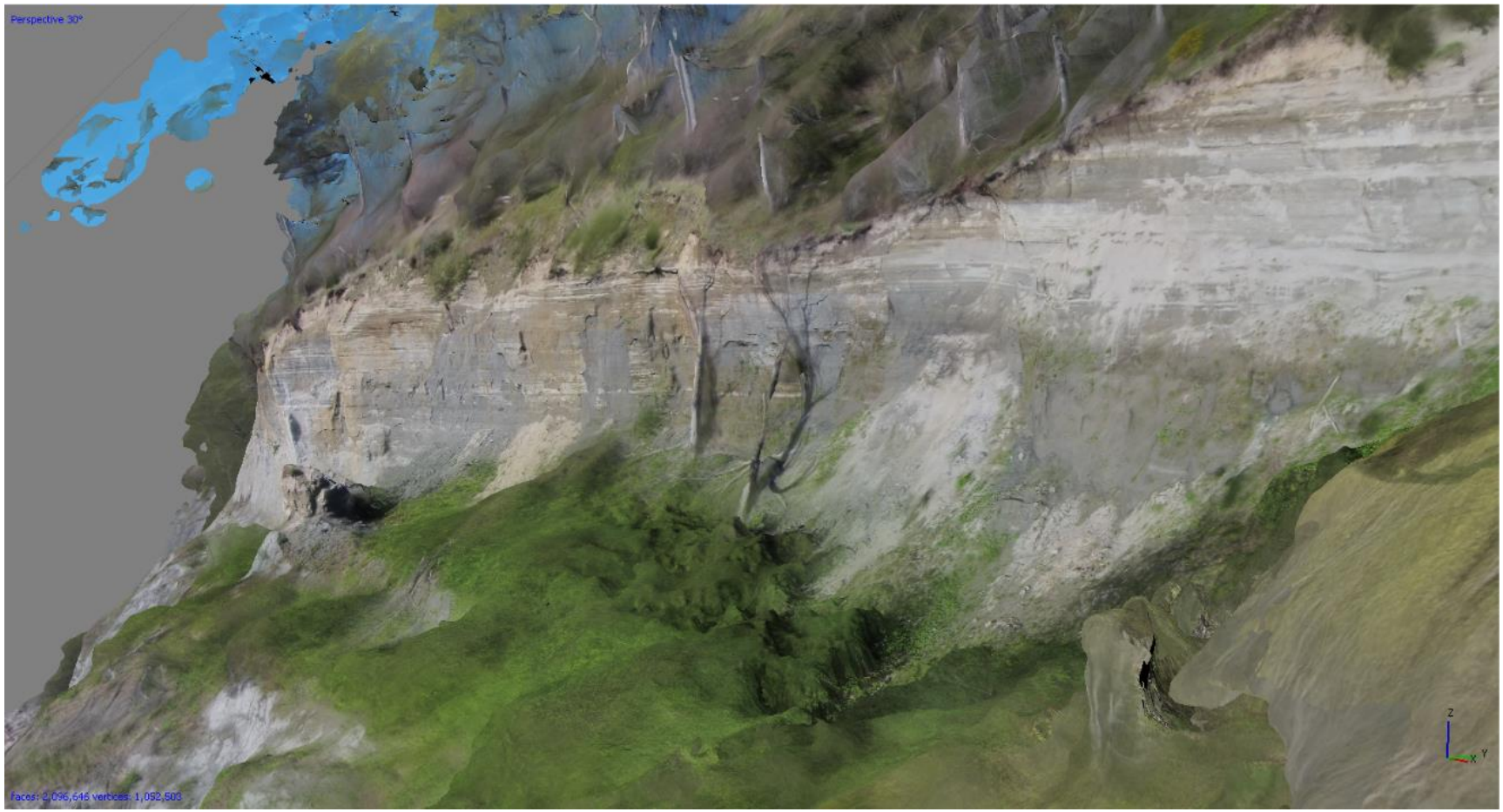

Angled view of SfM model, looking in the northwest direction.

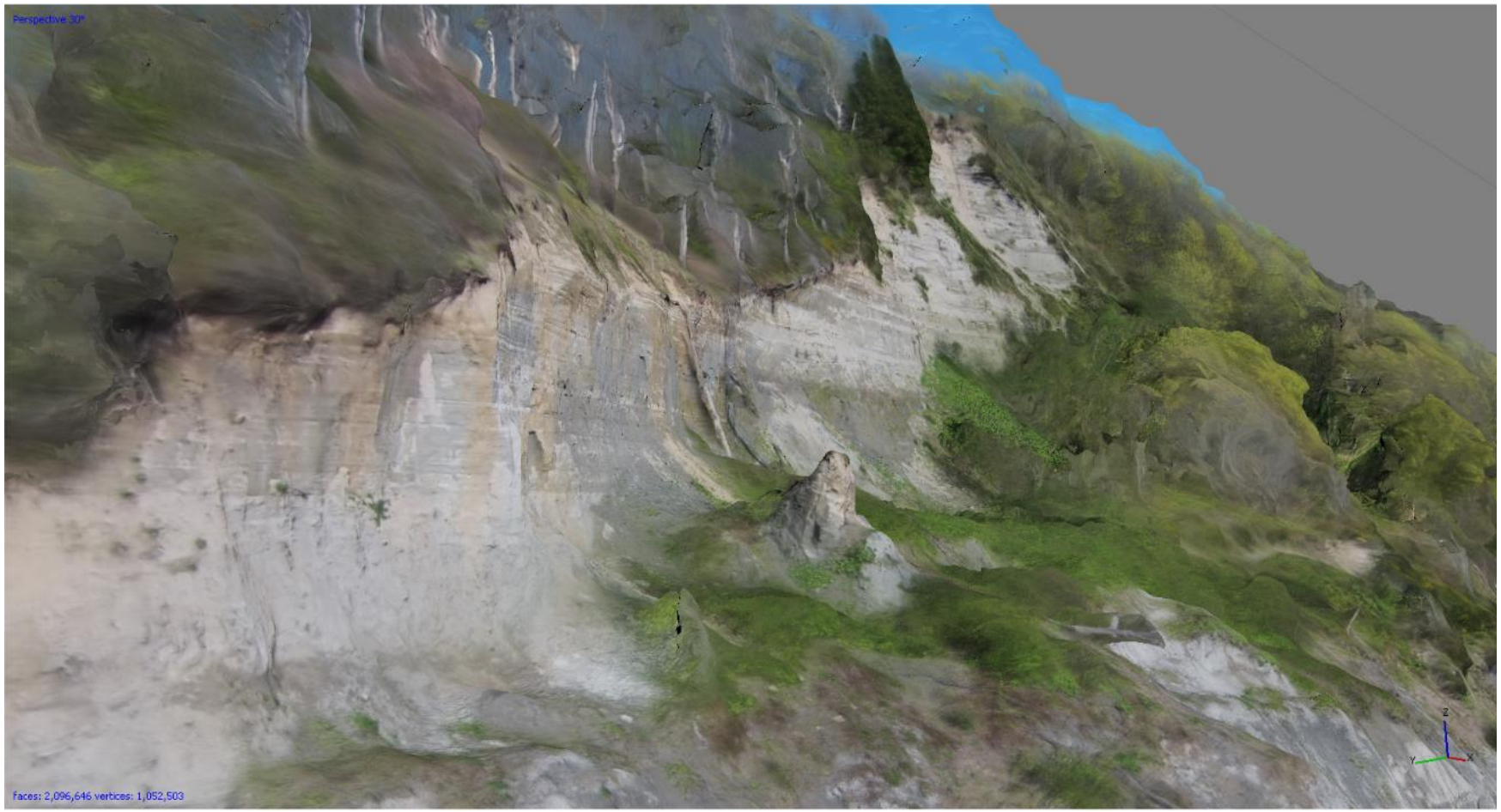

Angled view of SfM model, looking in the southeast direction.

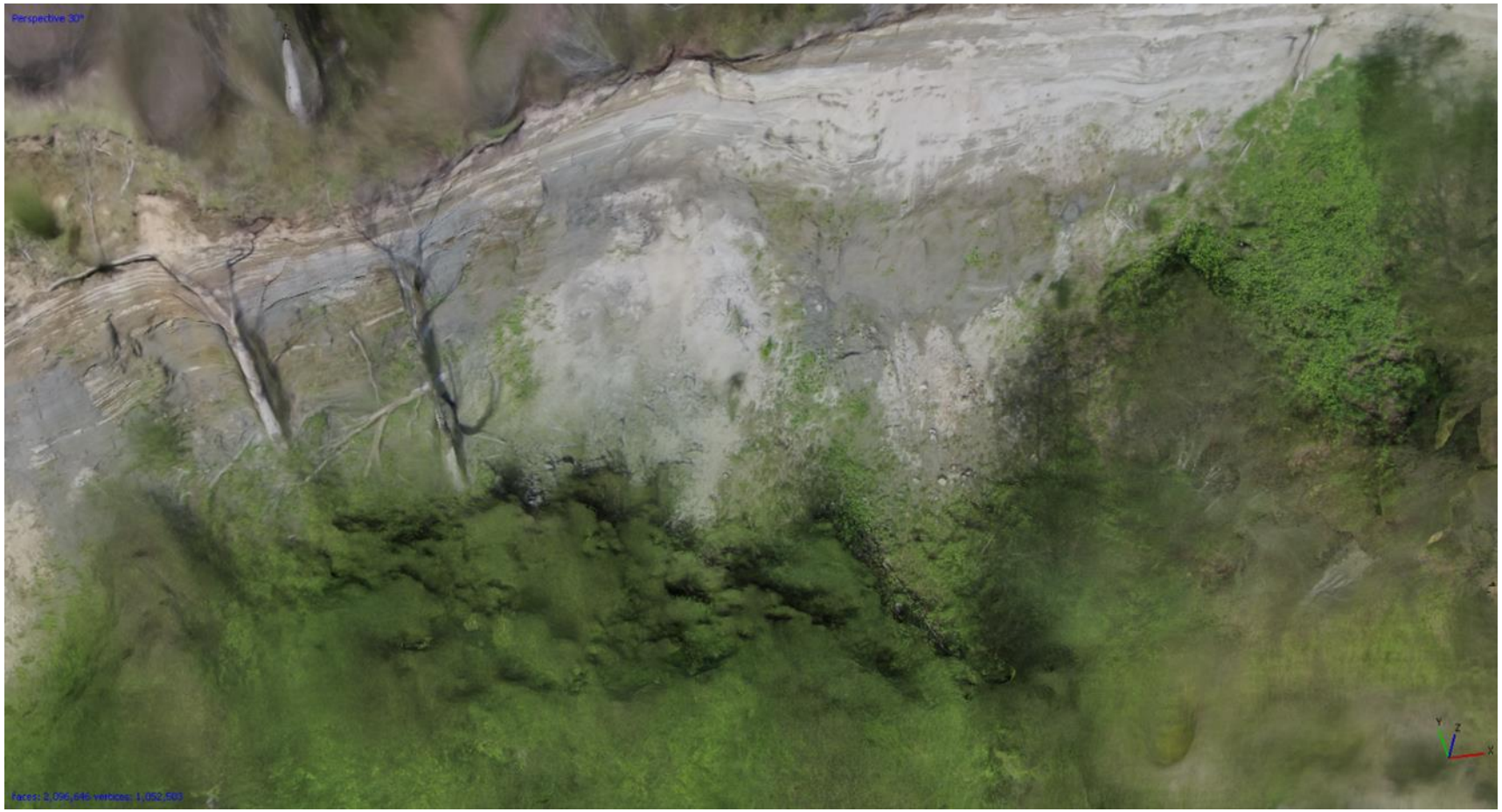

Close-up view of SfM model showing distinct shadows and vegetation blurring.